ACS Catalysis

RESEARCH ARTICLE

pubs.acs.org/acscatalysis

NO_x Storage and Reduction with H_2 on Pt/Rh/BaO/CeO_2: Effects of Rh and CeO_2 in the Absence and Presence of CO_2 and H_2O

Yongjie Ren and Michael P. Harold*

Department of Chemical and Biomolecular Engineering University of Houston Texas 77204-4404, United States

ABSTRACT: The storage and reduction features of a family of Pt/Rh/BaO/CeO_2/Al_2O_3 washcoated monolith catalysts are compared in terms of NO_x conversion and product selectivity using H_2 as the reductant. The catalyst composition, monolith temperature, regeneration time, and presence of H_2O and CO_2 in the feed were systematically varied to identify trends and to elucidate effects. In addition to cycling, experiments involving the reduction of a fixed amount of prestored NO_x help to isolate differences in the regeneration features of the catalysts. The addition of both CeO_2 and Rh to Pt/BaO increases the cycle-averaged NO_x conversion and selectivity to N_2, but oxygen storage on the ceria expectedly leads to the consumption of additional reductant during the regeneration. CeO_2 is shown to be an inferior NO_x storage component, but as a supplement to BaO, CeO_2 provides the role of promoting the oxidation of NH_3 to N_2. The same stored oxygen is the likely cause for the enhanced NH_3 oxidation. On the other hand, Pt/BaO is shown to be the most effective catalyst for converting NO_x to NH_3. Fixed NO_x storage experiments show the existence of at least three rate-controlling regimes: one that is reductant-feed-rate-limited, another that is limited by NO_x storage phase diffusion, and a third that has a chemical or textural origin. On Pt/BaO, the first two regimes are clearly distinguishable, whereas a more complex picture emerges for Pt/CeO_2, with which a fraction of the stored NO_x is kinetically inaccessible to reduction. Water inhibits the oxidation of NO on each catalyst, but the cycle-averaged NO_x conversion is largely unaffected. In contrast, CO_2 has only a minor effect on the conversion during steady state NO oxidation but significantly inhibits the NO_x conversion during cyclic storage and reduction. This effect is attributed to the known higher stability of $BaCO_3$ compared with $BaO/Ba(OH)_2$. The conversion of H_2 to the less effective reductant CO via reverse water gas shift chemistry is a contributing factor based on steady-state activity tests. This pathway is shown to be most important for the catalysts, containing Rh/CeO_2, a known effective water gas shift catalyst. Building on the existing literature, most of the observed trends are interpreted in terms of the likely reaction pathways and transport processes. The findings are assessed in terms of identifying the catalyst best suited to the specific NO_x trap application, be it a stand-alone reactor or one coupled with downstream NH_3-based selective catalytic reduction.

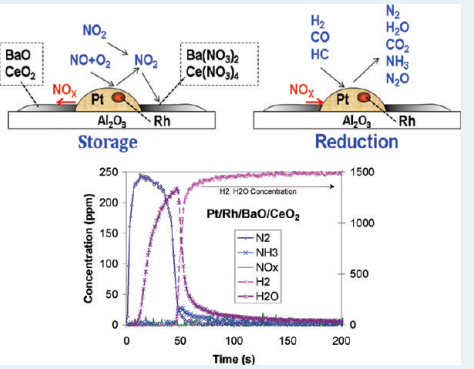

KEYWORDS: NO_x, hydrogen, platinum, lean NO_x trap, ceria, rhodium

INTRODUCTION

The storage and reduction of nitric oxide (NO) and nitrogen dioxide (NO_2), collectively known as NO_x, has emerged as an important emission aftertreatment process for light- and medium-duty lean burn gasoline and diesel engines. The main advantage of NO_x storage and reduction (NSR) is that the reductant source is the fuel, so there is no need to manage and supply urea required for NH_3-based selective catalytic reduction (SCR). NSR is also seeing application in combined NSR−SCR, which exploits the lower cost and durability of SCR catalysts on one hand and utilizes the NH_3 generation capabilities of NSR catalysts on the other. Most studies of the lean NO_x trap (LNT) to date have used NSR catalysts containing Pt and BaO. Pt is an effective NO oxidation and NO_x reduction catalyst, and BaO has excellent NO_x storage features, making Pt/BaO a good model catalyst to study various catalyst and reactor issues. An earlier review by Epling et al.[1] and more recent ones by Guthenke et al.[2] and Roy and Baiker[3] provide a thorough coverage of the developments in this important environmental abatement process.

In the past few years, a group of investigators have shown improved performance of the LNT by the addition of various catalytic and storage materials. In particular, ceria (CeO_2) provides superior sulfur resistance, stabilizes the precious metal dispersion, and improves the low-temperature NO_x storage and reduction performance over catalysts containing only the aforementioned BaO storage material. In addition, Rh in combination with CeO_2 comprises an excellent water gas shift (WGS) catalyst, which is a known pathway for generating additional H_2 in exhausts containing CO. Theis et al.[4] compared the WGS activity of catalysts containing ceria and different precious group metals. They found that Rh/CeO_2 was more active than Pt/CeO_2. In addition to its role for helping to promote WGS activity, Rh provides excellent NO bond scission activity, which should increase the regeneration activity.[5] Platinum is a reasonable NO_x reduction catalyst at higher temperatures, but it is inferior to Rh for NO_x reduction at lower temperatures (<250 °C).[4]

Received: May 15, 2011
Revised: June 24, 2011
Published: June 28, 2011

Indeed, one reason Rh was added to the catalytic converter during the early years of its development was to reduce the production of ammonia. Schlatter and Taylor[6] showed that Rh alone was effective in converting NO to N_2. The addition of Pt improved the oxidation performance and increased the level of NH_3. With its well-established role as an oxygen-storage material in the modern three-way catalytic converter, ceria helps to eliminate ammonia through the dynamic supply of oxygen during rich operation, conditions that would otherwise favor ammonia production. But the storage of oxygen is detrimental in the LNT because it leads to increased consumption of reductant during the regeneration. Moreover, ammonia is a desired product in the NSR/SCR application. So despite its advantages, ceria may not be a logical component in such applications.

Several studies of ceria have been carried out in recent years to understand its role during NSR. In most of these studies, ceria was an additive to the $Pt/BaO/Al_2O_3$ catalyst or a substitute for Al_2O_3. Theis et al.[7] were among the first to report the beneficial effects of ceria at low to moderate temperatures using feeds representative of vehicle exhaust. Ji et al.[8] showed for a series of powder catalysts the benefits of ceria, due in part to the fact that the stored NO_x in ceria-containing LNT catalysts has a lower thermal stability; this affords improved NO_x reduction at low to intermediate temperatures. This is likely due to the lower stability of NO_x stored on CeO_2. Ji et al.[9] carried out another systematic study of storage and reduction experiments on a series of Pt/Rh/Ba/Ce/Zr/La monolithic catalysts. The Pt/Rh loading and dispersion and BaO loading were fixed while the loadings of Al_2O_3, CeO_2, ZrO_2 were varied for a fixed overall washcoat loading. The NSR results show that the ceria-containing catalysts are more effective than the catalyst containing only BaO at low temperature (150 °C). The replacement of alumina by CeO_2 and ZrO_2 results in a higher cycle-averaged NO_x conversion. The investigators attributed the results to a "more facile decomposition" of the stored NO_x species on ceria. Ji et al.[10] also showed significantly enhanced oxygen storage as the ceria loading was increased. Casapu et al.[11] showed that $Pt/BaO/CeO_2$ is not as effective as $Pt/BaO/Al_2O_3$, particularly during the regeneration. They attributed the findings to both textural and chemical factors. For example, ceria's capacity to store oxygen competes with its capacity to store NO_x; this leads to oxidation of reductant rather than reduction of NO_x. Yoshida et al.[12] and Martin and Duprez[13] suggest that CeO_2 may enhance the formation of Pt oxides due to ceria's higher basicity. On the other hand, CeO_2 out-performed several other oxides (of Ti, Zr, Ce/Zr, Al) in terms of NO_x storage capacity. Schmeiβer et al.[14] compared Pt, Pt/CeO_2, Pt/BaO, $Pt/CeO_2/BaO$ and $Pt/Rh/CeO_2/BaO$ catalysts in terms of steady-state NO oxidation activity and NO reduction using reductant mixtures containing H_2, CO, and C_3H_6. Comparisons of cyclic performance were also carried out, although no NH_3 data were reported. Notwithstanding the potential production of H_2 by the water gas shift reaction (due to the presence of CO and H_2O), ceria's oxygen storage function reduces the net generation of NH_3. This is the result not only through NH_3 oxidation, but also through oxygen release, which maintains a stoichiometric air-to-fuel ratio, conditions that are less favorable for NH_3 formation. Ceria-containing LNT catalysts have a better overall combination of NO_x reduction to N_2 than their ceria-free counterparts.

The ubiquity of combustion products CO_2 and H_2O in vehicle exhaust emphasizes the importance of understanding their roles—beyond mere dilution—in affecting the performance of NO_x trap catalysts. An earlier study by Lietti et al.[15] showed that the presence of H_2O and CO_2 in the feed leads to a solid phase mixture of BaO, $Ba(OH)_2$, and $BaCO_3$. Although NO_x has the propensity to store on each of these materials, there are notable differences in the stabilities and corresponding NO_x storage capacities of these species. Epling et al.[16] showed that H_2O and CO_2 reduce the storage of NO_x. On the other hand, Theis et al.[17] showed that the total amount of stored NO_x increased in the presence of H_2O. They attributed this trend to enhanced spillover of NO_2 from Pt to the barium storage phase. These differences suggest that the details of the catalyst preparation and test procedures may lead to different conclusions. Lindholm et al.[18] carried out a study of Pt/Ba/Al, Pt/Al, and Pt/Si catalysts in which H_2 was the reductant in the presence of H_2O and CO_2. They showed the importance of the combustion products in affecting the overall NSR performance. In the absence of these species, alumina has a more active role as a NO_x storage material at lower temperatures. Notably, CO_2 affects NO_x storage on the barium phase more than does H_2O. This is due to the aforementioned stability of $BaCO_3$ compared to $Ba(OH)_2$. Another interesting finding was an apparent enhancement in NH_3 production by CO_2. The authors attributed this feature to the same increased stability of $BaCO_3$. That is, NH_3 that is formed upstream during regeneration reacts downstream because of the smaller amount of stored NO_x. Scholz et al.[19] have shown that above 250 °C, the water gas shift reaction is responsible for producing H_2 from CO + H_2O and the resulting reduction of stored NO_x. Lindholm et al.[20] included the effect of CO_2 in their detailed kinetic model of NSR, although the model did not include the reverse water gas shift reaction, which is potentially important at higher temperatures and concentrations of CO_2. Schmeisser et al.[21,22] developed a model for NSR in which the barium storage phase volume expansion during nitrate formation inhibited pore diffusion through pore blockage. Effects of CO_2 and H_2O in the feed were also included.

Despite the progress made in understanding the roles of NSR catalyst additives Rh and CeO_2 and combustion products CO_2 and H_2O, there remain unresolved issues. Although the use of feeds containing the two reductants H_2 and CO as well as combustion products H_2O and CO_2 is important to emulate real exhaust, simpler feeds devoid of H_2O and CO_2 enable an isolation of pertinent effects. Moreover, differences in the storage properties of BaO and CeO_2 warrant a more direct, one-to-one comparison, and whereas storage and reduction cycling enables a comparison of the overall performance of NSR catalysts, this approach complicates the identification of the limiting rate process because the rates of storage and regeneration are necessarily equal at the cyclic steady state. The emergence of the aforementioned NSR/SCR process in particular requires a closer examination of the generation and consumption of NH_3. Finally, the performance of catalysts containing Rh and ceria in the presence/absence of H_2O and CO_2 over a range of operating parameters, such as LNT temperature, regeneration duration, etc. is generally not known. Such studies are necessary if the LNT is to be designed optimally for the conventional NSR or NSR/SCR application.

To this end, the objective of this study is to quantify and elucidate the effects of Rh and CeO_2 during NO_x storage and reduction. A series of monolithic catalysts, each containing Pt and Al_2O_3, and having a range of loadings of Rh, BaO, and CeO_2 were studied in terms of NO oxidation, NO_x storage, and NO_x

Table 1. Washcoat Compositions of Pt/Rh/BaO/CeO_2 Catalyst Samples

wt %	Pt/BaO	Pt/BaO/CeO_2	Pt/Rh/CeO_2	Pt/Rh/BaO/CeO_2	Pt/CeO_2
Pt	2.36	2.36	2.36	2.36	2.36
Rh	0	0	0.17	0.17	0
BaO	12.7	12.7	12.7	12.7	0
CeO_2	0	12.7	0	12.7	12.7

storage and reduction activity. To our knowledge, this study is the most comprehensive comparison of several NSR catalyst components that includes the effects of CO_2 and H_2O and which focuses on net generation of NH_3. The effects of Rh and CeO_2 are also evaluated both without and with CO_2 and H_2O in the feed to isolate specific effects. Both cycle-averaged NSR and fixed NO_x storage and regeneration experiments are used to assess the balance between storage and reduction for the former and regeneration kinetics for the latter. More detailed experiments are carried out to compare the features of BaO and CeO_2 in affecting storage and reduction. Mechanistic reaction pathways and rate-controlling processes are proposed to explain the main trends in the data.

EXPERIMENTAL SECTION

Catalyst Samples. The Pt/Rh/BaO/CeO_2 series of monolith catalysts were provided by BASF Catalysts (Iselin, New Jersey). The compositions of the washcoats are provided in Table 1. The monolith supports had a cordierite structure (62 channels/cm^2) and a high-surface-area γ-Al_2O_3 washcoat containing active precious metal (Pt, Rh, or both) and metal oxides (BaO, CeO_2, or both). The Pt loading was fixed at 96 g/ft^3 for all samples, and when present, the Rh loading was 6.8 g/ft^3. The total washcoat loading was 2.3 g/in^3 for all samples; the incremental loadings of BaO and CeO_2 were 0.3 g/in^3, when present. Thus, both the BaO and CeO_2 replaced equivalent amounts of Al_2O_3 filler. The catalyst samples were cut into nearly cylindrical cross sections of ~0.8 cm diameter and 2 cm length and had 28 channels in cross section. The mass of washcoat (m_{wc}) for each monolith sample was ~130 mg. Unless otherwise noted, the catalysts were slightly aged before exposure to a flowing gas mixture at 400 °C with a composition of 500 ppm NO, 5% O_2, and 2% H_2 for 2 h. Subsequent efforts were made to maintain a constant activity over the course of the study by avoiding temperature excursions above 450 °C. Some of the data were obtained with fresh catalyst and are so indicated.

Reactor Setup. The experimental setup comprising a vertical downflow reactor is the same as that described previously.[23,24] Two gas streams, corresponding to the net lean and rich feeds, were alternatively introduced into the reactor through an electronically controlled switching valve located just upstream of the reactor. Individual components or binary mixtures were metered by high-precision mass flow controllers. The total volumetric flow rate through the reactor was 1000 standard cm^3 per minute (GHSV = 60 000 h^{-1} at 273.15 K and 1 atm). The monolith catalysts were wrapped in Fiberfrax ceramic paper to prevent any bypassing around the catalyst during the experiments. The temperature of the catalyst was measured by a sheathed K-type (0.5 mm o.d.) thermocouple, which was positioned in a monolith channel at the approximate midpoint of the monolith (axial and radial). The effluent from the reactor

Table 2. Flow Conditions Used in the Experiments

component	storage phase (lean)	regeneration phase (rich)
NO	500 ppm	0
O_2	5%	0
H_2	0	5000 ppm
CO_2	0 or 5%	0 or 5%
H_2O	0 or 5%	0 or 5%
Ar	balance	balance
duration	60s	30 s

was monitored and analyzed using a FT-IR spectrometer (Thermo-Nicolet Nexus 470), with which the concentration of species, including NO, NO_2, NH_3, N_2O, CO, CO_2, and H_2O, were recorded. A quadrupole mass spectrometer equipped with a capillary probe quantified the N_2 and H_2 in the effluent. In all of the experiments, argon was used as the diluent. The sampling rate through the capillary was ~30 sccm.

When steam was introduced into the system, liquid water was first injected into an evaporator by a high precision pump (Isco model 5000), then the evaporated steam was carried by balance gas argon and entered the reactor though the entrance located just downstream from the switching valve.

NO Oxidation Experiments. The NO oxidation activities of the Pt/Rh/BaO/CeO_2 catalyst family were compared to assess potential effects on their storage and reduction performance. Steady-state NO oxidation was carried out by flowing a 500 ppm NO, 5% O_2 with and without H_2O and CO_2 between 150 and 400 °C. The NO conversion was calculated using

$$X_{NO} = \frac{[NO_2]}{[NO_2] + [NO]} \times 100 \quad (1)$$

Acknowledging that this reaction system can lead to the undesired oxidation of Pt crystallites,[25] care was taken to ensure that a steady-state was obtained based on <1% variation in the outlet composition for ~30 min.

NO_x Storage Experiments. The storage of NO_x was measured under cycling conditions for which the reductant H_2 was in excess of stoichiometric requirements to convert all the NO feed. This ensured that the catalyst was regenerated prior to feeding a mixture containing 500 ppm NO; 5% O_2; and, in some experiments, H_2O, CO_2, or both. Two quantities of interest included the NO_x trapping efficiency, η_T, defined by[23]

$$\eta_T = 100\left(1 - \frac{1}{t^* F^o_{NO_x}} \int_0^{t^*} F_{NO_x}(t)\, dt\right) \quad (2)$$

where t^* is the duration. The NO_x storage concentration, C_{NO_x}, is defined by

$$C_{NO_x} = \eta_T F^o_{NO_x} t^* / 100 m_{wc} \quad (3)$$

where m_{wc} is the mass of the washcoat.

Lean and Rich Cycling Experiments. The cycling experiments involved an alternating lean−rich procedure. The lean and rich phase compositions are provided in Table 2. These experiments were carried out over a wide temperature range (150−400 °C). The experiment was started at the lowest temperature, and once a cyclic steady-state was reached, the product compositions were recorded. Then the temperature was

dx.doi.org/10.1021/cs200252r |ACS Catal. 2011, 1, 969–988

increased to the next set point at a ramp of 25 °C/min. The procedure was repeated until all of the prescribed temperatures were accessed. Unless otherwise stated, the total cycle time was 90 s, with 60-s lean and 30-s rich phases.

Several performance variables are of interest. The cycle-averaged NO_x and H_2 conversions are given by

$$X_{NO_x} = \frac{\int_0^{t_{S+R}} \left[F^o_{NO}(t) - F_{NO_x}(t)\right] dt}{\int_0^{t_{S+R}} F^o_{NO}(t)\, dt}$$

$$X_{H_2} = \frac{\int_0^{t_{S+R}} \left[F^o_{H_2}(t) - F_{H_2}(t)\right] dt}{\int_0^{t_{S+R}} F^o_{H_2}(t)\, dt} \quad (4)$$

where t_{S+R} is the time for one complete storage (S) and reduction (R) cycle (s). F^o_i (mol/s) is the feed rate of species i, and F_i (mol/s) is the effluent molar flow rate of species i. The cycle-averaged NH_3, N_2, and N_2O selectivities are calculated using[24,26]

$$S_i = \frac{\int_0^{t_{S+R}} F_i(t)\, dt}{\int_0^{t_{S+R}} \left[F^o_{NO}(t) - F_{NO_x}(t)\right] dt}$$

$$F_i \equiv F_{NH_3}, 2F_{N_2}, 2F_{N_2O} \quad (5)$$

The "dynamic" stored NO_x (mol/g washcoat) is calculated by

$$NO_x^{stored}(t_s) = \frac{\int_0^{t_S} \left[F^o_{NO} - F_{NO_x}(t)\right] dt}{m_{wc}} \quad (6)$$

where t_s is the storage time (s) and m_{wc} is the mass of the washcoat (g).

A systematic variation in the rich phase duration was carried out to span a range of cycle-averaged conversions of the NO_x and H_2. The regeneration time was varied from 5 to 30 s, while the storage time was fixed at 60 s. Particular attention was placed on identifying the rich time for which the NO_x and reductant conversions simultaneously exceeded 80%.

Fixed Storage Experiments. In the regeneration procedure, the reductant reacts with the stored NO_x and in so doing cleans the storage sites for the next NO_x trapping step. The fixed storage experiment was designed to explore the regeneration procedure and understand more about the mechanism of regeneration of stored NO_x.[27] The amount of NO_x stored with a feed of 500 ppm NO and 5% O_2 in Ar was fixed at $\sim 1.65 \times 10^{-5}$ mol (within 3% deviation) for each NO_x storage experiment. The catalyst was first pretreated at 425 °C in 1500 ppm H_2 until H_2O and NH_3 were not observed in the effluent, then a 5 min Ar purge was carried out to remove any species accumulated on the catalyst. [Remark: To avoid Pt sintering, the pretreatment temperature was limited to 425 °C.] After this pretreatment, the catalyst sample was cooled to the desired temperature in a flow of Ar. So-called "pre-storage" experiments were carried out using a feed of 500 ppm NO and 5% O_2 prior to the fixed storage experiments. The prestorage experiments were intended to determine the storage time needed to achieve a prescribed value at each temperature and catalyst sample. The duration of the prestorage process was determined to give the prescribed 1.65×10^{-5} mol of stored NO_x according to

$$stored\ NO_x = \int_0^{t_S} \left[F^o_{NO} - F_{NO_x}(t) - 2\left(F_{N_2O}(t) + F_{N_2}(t)\right)\right] dt \quad (7)$$

This procedure (pretreatment and prestorage) was repeated at six temperatures (150, 200, 250, 300, 350, and 400 °C) for each of the catalyst samples.

After the storage times were determined, the catalysts were again pretreated and cooled in flowing Ar to the desired temperature. A series of fixed-storage regenerations were then conducted. Once NO_x was stored, the regeneration was initiated by promptly switching to a feed containing 1500 ppm H_2. The regeneration was carried out for 15 min (900 s), which was sufficient time to ensure no H_2O or NH_3 in the effluent. Then a pretreatment was conducted for the next fixed-storage experiment. During the pretreatment, the amount of unreacted NO_x from the previous run, (N^{acc}), was estimated from the evolved ammonia according to

$$[N^{acc}] = \int_0^{t_{pre}} \left[F_{NH_3}(t)\right] dt \quad (8)$$

where t_{pre} is the pretreatment time. Since the fixed stored NO_x experiments involved only one cycle, the NO_x conversion is based on the amount of the initial stored NO_x as calculated from eq 9 below. The instantaneous stored NO_x conversion at time t^* during the regeneration is calculated from the species exiting the monolith by

$$X_{NO_x stored} = \frac{\int_0^{t^*} \left[F_{NH_3}(t) + 2\left(F_{N_2O}(t) + F_{N_2}(t)\right)\right] dt}{\int_0^{t_S} \left[F^o_{NO} - F_{NO_x}(t) - 2\left(F_{N_2O}(t) + F_{N_2}(t)\right)\right] dt} \quad (9)$$

where t^* is the time during regeneration (s), spanning 0 to t_R. Unreacted NO_x that is released in the form of NO and NO_2, the so-called "NO_x puff", is not included in the numerator. The denominator is the amount of NO_x stored (in moles). The corresponding selectivities over the entire regeneration are defined as

$$S_i = \frac{\int_0^{t_R} F_{NO_x}(t)\, dt}{\int_0^{t_R} \left[F_{NO_x}(t) + F_{NH_3}(t) + 2\left(F_{N_2O}(t) + F_{N_2}(t)\right)\right] dt + [N^{acc}]} (100\%)$$

$$F_i \equiv F_{NO_x}, F_{NH_3}, 2F_{N_2O}, 2F_{N_2} \quad (10)$$

$$S_{NH_3} = \frac{\int_0^{t_R} F_{NH_3}(t)\, dt}{\int_0^{t_R} \left[F_{NO_x}(t) + F_{NH_3}(t) + 2\left(F_{N_2O}(t) + F_{N_2}(t)\right)\right] dt + [N^{acc}]} (100\%) \quad (11)$$

RESULTS

NO Oxidation. The oxidation of NO may be the rate-limiting process, depending on the overall reductant/NO_x ratio, so measuring the NO oxidation activity is clearly relevant. Figure 1

dx.doi.org/10.1021/cs200252r |ACS Catal. 2011, 1, 969–988

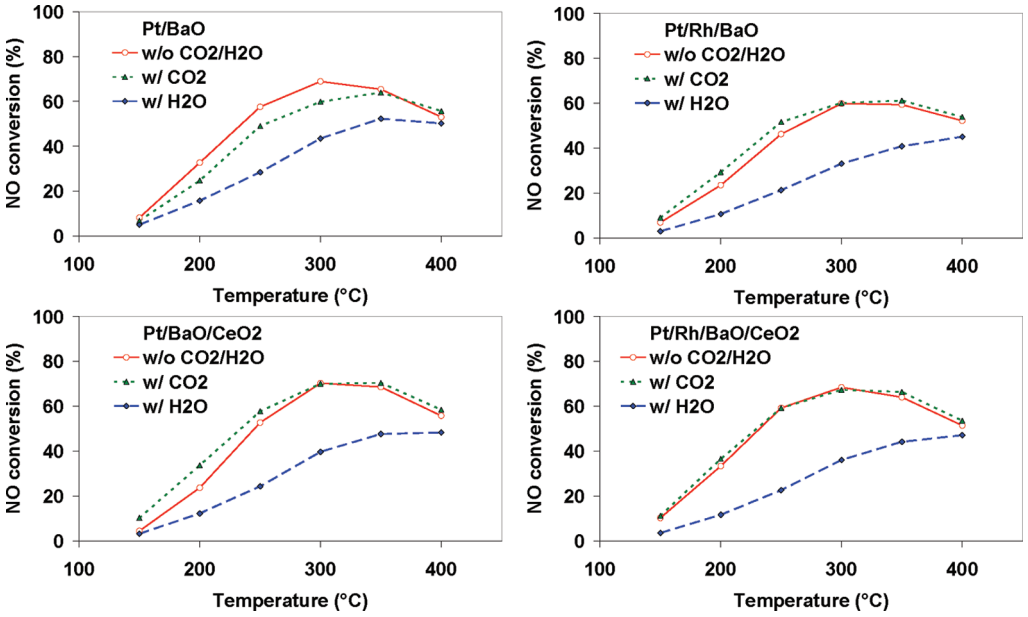

Figure 1. NO conversion as a function of monolith temperature during steady-state NO oxidation on the catalysts (fresh). The feed contains 500 ppm NO, 5% O_2, and balance Ar.

shows the dependence of the steady-state conversion of NO to NO_2 without H_2O/CO_2, with H_2O, and with CO_2 for the Pt/Rh/BaO/CeO_2 catalysts. In the absence of H_2O or CO_2 in the feed, the maximum conversion occurred at about 300 °C. The decrease at higher temperature is a result of the shift to an equilibrium-limited regime.[28−30] The maximum NO conversion was 68−70% for all of the catalysts except Pt/Rh/BaO, which gave a conversion of 60%. The addition of CeO_2 reduced the conversion slightly at all temperatures except when CO_2 was in the feed. In that case, CeO_2 enhanced the NO oxidation rate. The effect of H_2O reduced the conversion more significantly at all temperatures and for all the catalysts, in agreement with the literature (e.g., ref 17). The effect of CO_2 was much less and led to either an increase or decrease in the conversion. On Pt/BaO, CO_2 inhibited the NO oxidation whereas on Pt/BaO/CeO_2, CO_2 promoted the NO oxidation at lower temperatures (<300 °C).

Storage and Reduction Cycling. As mentioned above, the H_2/NO_x ratio is an important parameter affecting the overall performance of the LNT. Figure 2 shows the dependence of the concentration of stored NO_x on the monolith temperature under cycling conditions (calculated using eqs 8 and 4). It is convenient to define the hydrogen to NO_x ratio as

$$\mathrm{H/N} = \frac{2 \times [\mathrm{H_2}] \times \tau_R}{[\mathrm{NO}] \times \tau_S} \qquad (12)$$

where τ_S and τ_R are the durations of the storage and reduction steps, respectively, and $[H_2]$ and [NO] are the feed concentrations of H_2 and NO, respectively. The storage measurements were done following the conditions in Table 2 ($[H_2]$ = 5000 ppm, [NO] = 500 ppm, τ_R = 30 s, τ_S = 60 s), giving H/N = 10. Since H/N = 5 corresponds to reduction of $Ba(NO_3)_2$ to N_2, the H/N = 10 feed is net-reducing. This ensured that the catalyst was mostly, if not completely, regenerated (to BaO, $Ba(OH)_2$, $BaCO_3$) before the next NO/O_2 storage cycle. Indeed, there was negligible breakthrough of NO or NO_2, and the NO_x conversion approached 100%. At lower temperature (150 °C), 0.15 mmol NO_x/g wc stored on Pt/BaO, which is about 87% of the total NO_x fed during the 60 s storage. An increase in temperature to 350 °C resulted in 99% of the NO_x feed being trapped on all four catalysts. The minor variation with temperature underscores that under these conditions, the NO_x storage was in a supply-limited state.

The data showed only a minor variation in the NO_x storage across the four catalysts when the feed was devoid of CO_2. The addition of 5% H_2O to the feed led to a slight increase in the storage at low temperature for each of the catalysts except for the fully formulated Pt/Rh/BaO/CeO_2. For example, at 150 °C, increases of 7%, 3%, and 4% for Pt/BaO, Pt/BaO/CeO_2, and Pt/Rh/BaO, respectively, were obtained. The enhancement diminished with increasing temperature, with the effect of H_2O actually becoming slightly inhibitive for T > 250 °C.

The addition of CO_2 resulted in a more significant effect on the NO_x storage and NO_x conversion. The fractional decrease was largest at the low temperatures. At 150 °C, the NO_x storage decreased over 40% to 0.085 mmol/g wc on the Pt/BaO. At 200 °C, an interesting, reproducible local minimum in the storage was observed for each of the catalysts except Pt/Rh/BaO/CeO_2. At higher temperatures, the inhibitive effect of CO_2 diminished for all of the catalysts.

The NO_x conversion was highest for all of the catalysts in the absence of H_2O/CO_2. The NO_x conversion increased with the addition of Rh and CeO_2. For example, the NO_x conversion was about 82% (99%) at 150 °C (350 °C) for Pt/BaO and about 92% (100%) at 150 °C (350 °C) for Pt/Rh/BaO/CeO_2. The addition of CO_2 resulted in a reduction, mirroring the decrease in the NO_x storage due to CO_2 addition.

The product distribution results in Figures 3 and 4 show that the main N-containing products are N_2, N_2O, and NH_3, in line with most previous works. Generally consistent trends with temperature were obtained for all of the catalysts. The cycle-averaged N_2 selectivity increased with temperature. For example, for Pt/BaO in the absence of feed CO_2 and

dx.doi.org/10.1021/cs200252r |ACS Catal. 2011, 1, 969–988

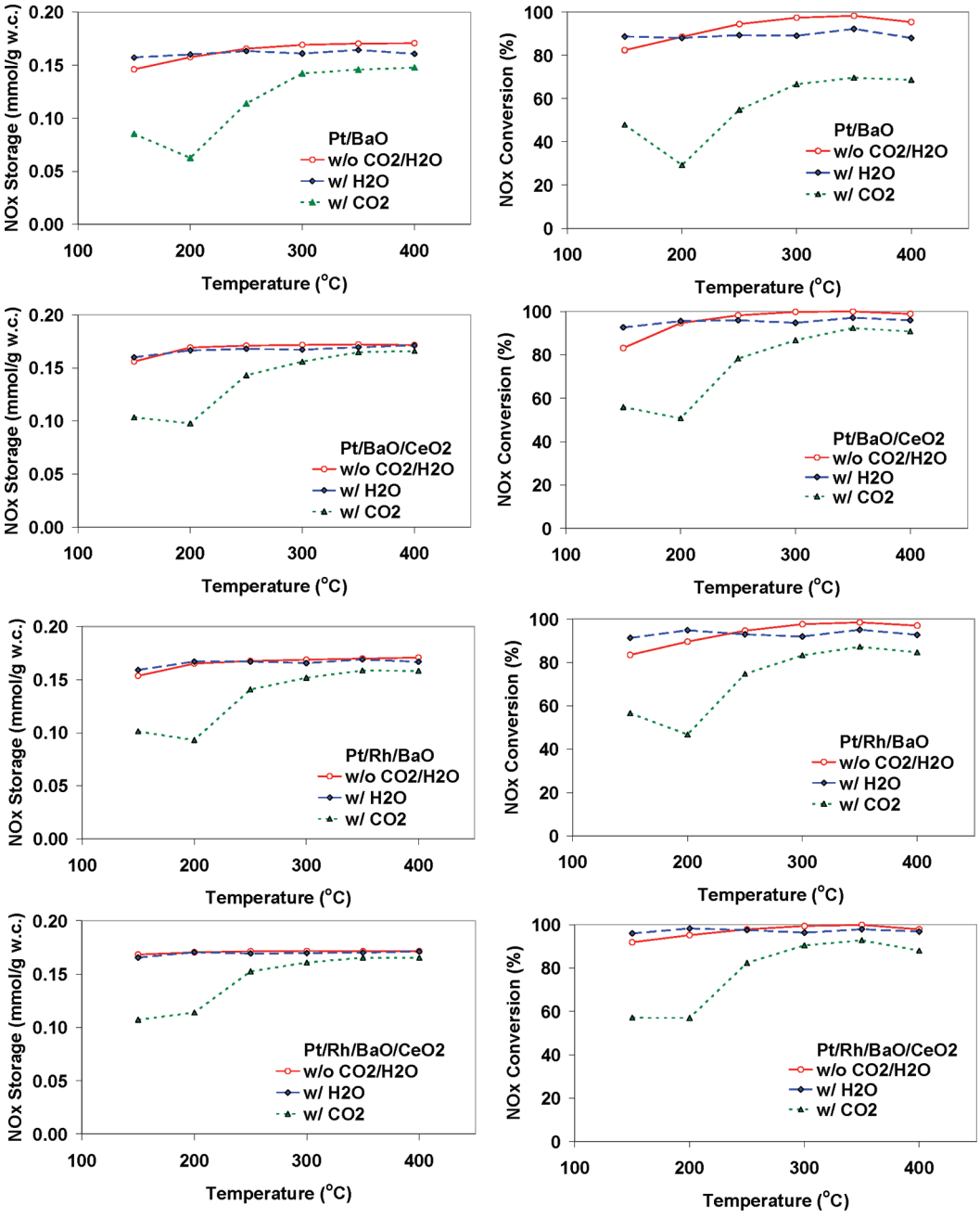

Figure 2. Cycle-averaged NO_x storage (left column) and NO_x conversion (right column) as a function of monolith temperature during cyclic storage and reduction on the fresh catalysts. Results are compared for feed devoid of CO_2/H_2O, and containing either 5% H_2O or 5% CO_2. The lean feed (60 s) contains 500 ppm NO and 5% O_2, and the rich feed (30 s) contains 5000 ppm H_2 and balance Ar.

H_2O, the N_2 selectivity was as low as 25% at 150 °C, increased to 91% at 300 °C, and was 96% at 400 °C. In comparison, the selectivity of N_2 reached 98% for the CeO_2-containing catalysts; that is, Pt/BaO/CeO_2 and Pt/Rh/BaO/CeO_2. The increase in N_2 selectivity with temperature came at the expense of N_2O and NH_3 selectivity, both of which achieved their highest values in the 150−200 °C temperature range. For temperatures exceeding 300 °C, the NH_3 selectivity decreased to less than 10%, and the N_2O was negligible for all four catalysts. For feeds devoid of CO_2, NH_3 was the favored product at the lowest temperature (150 °C), approaching 55% for Pt/BaO.

The effects of H_2O and CO_2 on the product distributions are also shown in Figures 3 and 4. In general, the N_2 selectivity decreased with the addition of H_2O, with the effect being larger at lower temperatures. The lone exception was the Pt/BaO/CeO_2 catalyst at lower temperatures, for which a slight increase in the N_2 selectivity was observed with the addition of H_2O. Most of the change in the N_2 selectivity was reflected as an opposite change in the NH_3 selectivity. Generally, the NH_3 (N_2O) selectivity increased (decreased) with the addition of H_2O. Again, the lone exception to this H_2O effect was Pt/BaO/CeO_2, which had a minor decrease in the NH_3 selectivity at lower temperature.

dx.doi.org/10.1021/cs200252r |*ACS Catal.* 2011, 1, 969–988

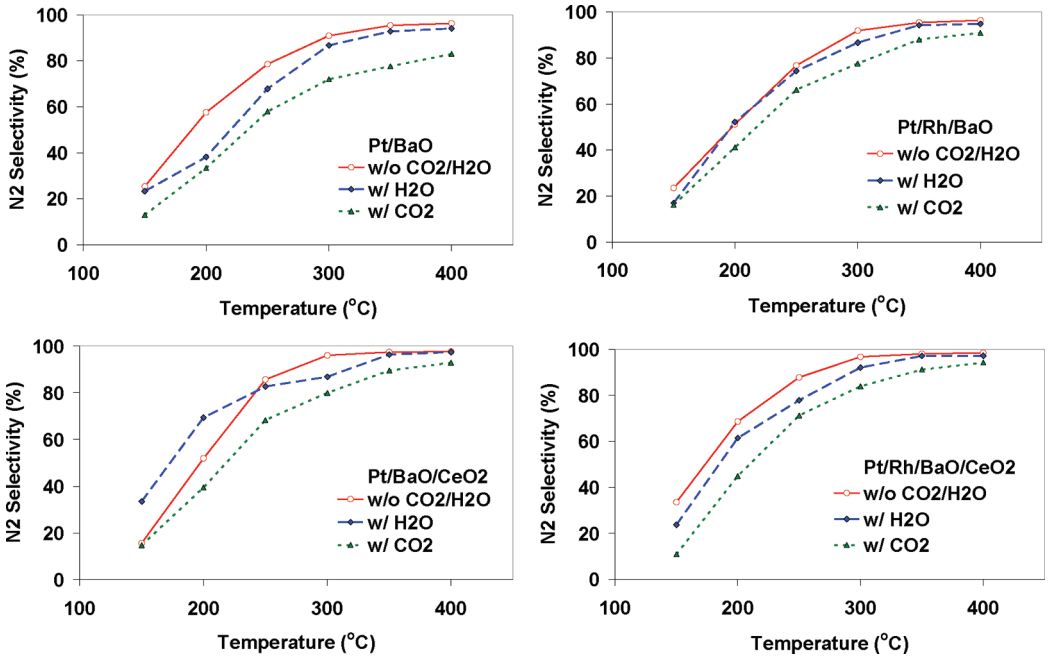

Figure 3. Cycle-averaged N_2 selectivity as a function of monolith temperature during cyclic storage and reduction on the fresh catalysts. Results are compared for feed devoid of CO_2/H_2O and containing either 5% H_2O or 5% CO_2. The lean feed (60 s) contains 500 ppm NO, 5% O_2; the rich feed (30 s) contains 5000 ppm H_2 and balance Ar.

In contrast to H_2O, CO_2 had an inhibitive effect on the NH_3 selectivity at lower temperature, with the main consequence being an increase in the N_2O selectivity. This trend was especially evident for the Pt/BaO. On the other hand, at temperatures above 250 °C, higher NH_3 selectivity was obtained when the feed contained CO_2. The N_2O selectivity converged gradually to the selectivity without CO_2 in the feed. Figure 5 shows the inhibitive effect of CO_2 on the catalyst performance over several initial storage-reduction cycles on the Pt/BaO catalyst (60 s storage, 30 s reduction). With 5% CO_2 in the feed, the breakthrough of NO_x was much more pronounced at 150 and 350 °C.

Over the entire temperature range studied (150−400 °C), an inhibitive effect of CO_2 on cycle-averaged NO_x conversion was observed for all of the catalysts. One potential factor contributing to this trend is the conversion of the H_2 reductant to CO by reverse water gas shift chemistry. According to Breen et al.[31] and others,[32−34] CO is a less effective reductant than H_2. To elucidate trends with CO_2 in the feed, we investigated the reactivity of CO_2 with H_2; that is, the reverse water gas shift reaction (rWGS):

$$CO_2 + H_2 \leftrightarrow H_2O + CO \qquad (R1)$$

Steady-state experiments of the rWGS reaction quantified the CO formation by flowing 5% CO_2 and 5000 ppm H_2 over each of the four catalysts. The steady-state conversions are shown in Figure 6. Differences in the conversions obtained from the four catalysts indicate that the forward endothermic reaction is not limited by equilibrium. At temperatures below 200 °C, the conversion was negligible, but above 300 °C, the conversion exceeded 10%. A conversion of 50% was achieved on the Pt/Rh/BaO/CeO_2 catalyst at 400 °C. The activity of the catalysts is in the order Pt/Rh/BaO/CeO_2 > Pt/Rh/BaO > Pt/BaO > Pt/BaO/CeO_2. Collectively, these data suggest that the conversion of H_2 to CO helps to explain the decrease in NO_x conversion with the addition of CO_2 and that the addition of the Rh and CeO_2 promotes this pathway.

Variation of Regeneration Time. The cycling data reported so far involved excess reductant, storage-limited conditions; specifically, H/N = 10. A variation in the regeneration time spanning a wide range of H/N values enables an assessment of effects when the balance shifts to regeneration-limited conditions. Figure 7 compares for the Pt/Rh/BaO/CeO_2 catalyst the cyclic steady state effluent concentrations of all the main reactant and product species for several different regeneration times between 5 and 30 s and T = 350 °C. The rather long purges reflect the low H_2 feed concentration of 0.5% v/v. The corresponding cycle-averaged conversion and product selectivity data are provided in Figure 8. The integral data clearly show the demarcation between the two limiting regimes, and the product profiles show more detailed transient effects. For a fixed storage time and temperature, the reductant conversion is complete at sufficiently low regeneration times, whereas at high regeneration times, the NO_x conversion approaches an asymptotic limit. At an intermediate regeneration time, the reductant and NO_x conversions intersect. This intersection point is a practical criterion for assessing a particular catalyst. The data show that the addition of Rh and CeO_2 serves to increase the conversion at the intersection point. In fact, for the Pt/Rh/BaO/CeO_2 catalyst, the cycle-averaged conversion is nearly 100%. The reductant conversion to achieve a prescribed NO_x conversion is higher for the ceria-containing catalysts. For example, to achieve a NO_x conversion of 90%, the H_2 conversion is about 87−88% for the Pt/BaO catalyst but approaches 98% for the Pt/BaO/CeO_2 catalyst.

The transient concentration profiles for the Pt/BaO catalyst have distinguishing features that reflect the relative supplies of stored NO_x and reductant (Figure 8). In the reductant-limited regime (τ_R < 20 s) the notable features include the breakthrough of NO_x during the storage, the so-called "NO_x puff" at the beginning of the regeneration, and the absence of any

dx.doi.org/10.1021/cs200252r |ACS Catal. 2011, 1, 969–988

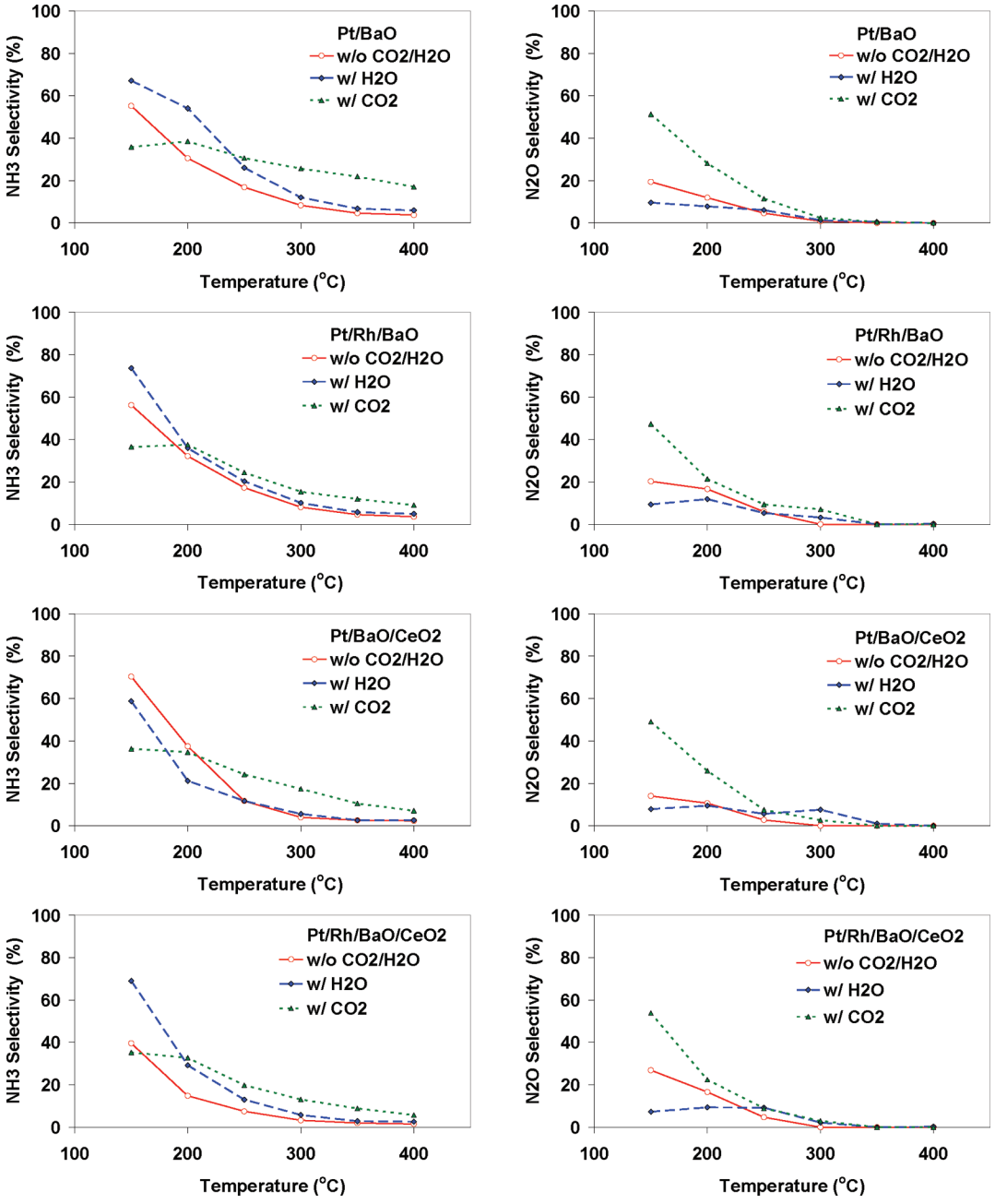

Figure 4. Cycle-averaged NH_3 selectivity (left column) and cycle-averaged N_2O selectivity (right column) as a function of monolith temperature during cyclic storage and reduction on the fresh catalysts. Results are compared for feed devoid of CO_2/H_2O, and containing either 5% H_2O or 5% CO_2. The lean feed contained 500 ppm NO and 5% O_2; the rich feed contained 5000 ppm H_2 and balance Ar.

unreacted H_2 or of NH_3 during the regeneration. For progressively shorter regenerations, the NO_x breakthrough becomes more pronounced. Storage sites are not completely regenerated, and storage becomes more difficult. For shorter regeneration times, a larger amount of NO_x accumulates on the catalyst, and storage is less efficient, and more NO_x is released during regeneration. Exacerbating the situation is the reaction between stored oxygen and reductants.[35] Although the regenerations are anaerobic (no gas phase O_2), heat is released because of the oxygen release from ceria and reaction. The temperature rise increases, and as a result, more NO_x able to store at the higher temperature. The small but measurable N_2O generated reflects the favorable, low H/N conditions for its formation. The absence of NH_3 in the product suggests that there is ample NO_x stored downstream that is available to react with NH_3 produced upstream in the reactor. In the NO_x-limited regime (τ_R > 20 s), the notable features include (i) the absence of any NO_x breaking through during the storage or regeneration, (ii) the breakthrough of unreacted H_2, (iii) the lack of any N_2O, (iv) the generation of NH_3, and (v) the comparatively large N_2 and H_2O peaks. The NH_3 appears at essentially the same time that breakthrough of unreacted H_2 appears, underscoring the fact that the accessible stored NO_x has been depleted.

dx.doi.org/10.1021/cs200252r |*ACS Catal.* 2011, 1, 969–988

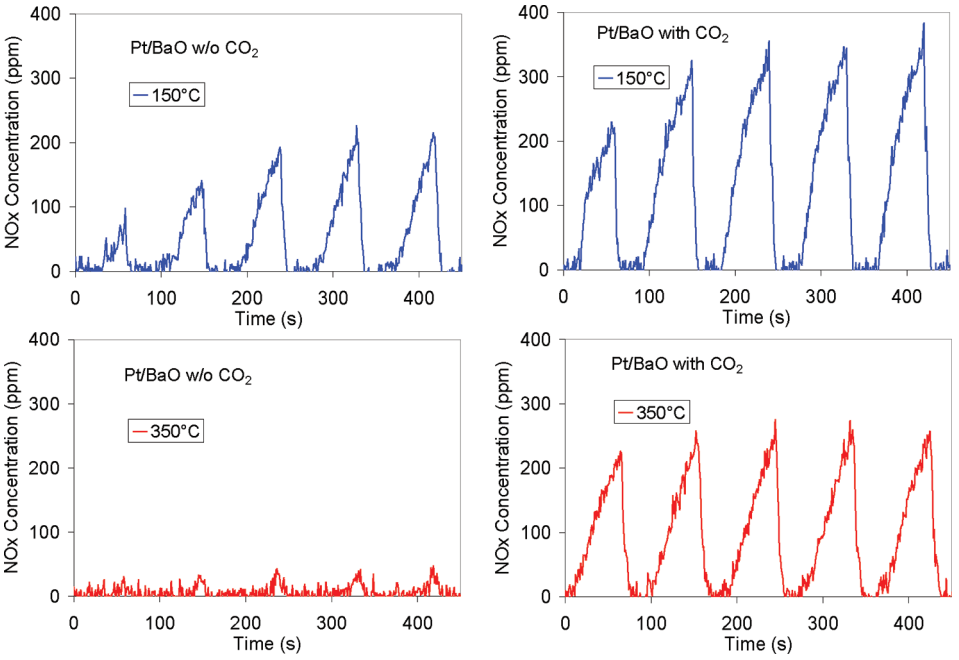

Figure 5. Typical approach to cyclic steady-state for the total NO_x concentration. The catalyst is fresh Pt/BaO, temperatures are 150 °C (top panels) and 350 °C (bottom panels), and the feed is either devoid of CO_2 (left panels) or contains 5% CO_2 (right panels). The cycling involved a lean phase duration of 60 s and rich phase duration of 30 s.

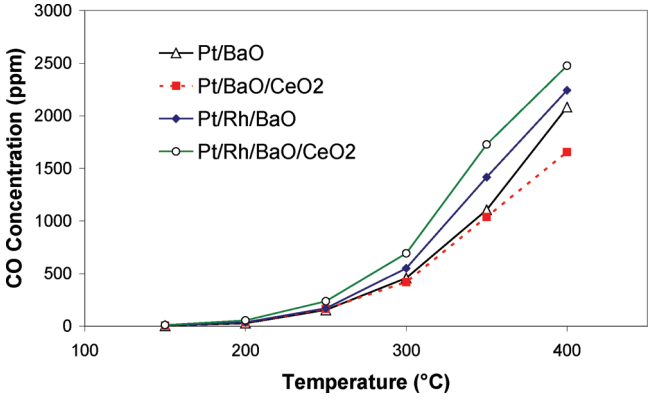

Figure 6. Dependence of effluent CO concentration on catalyst temperature during reverse water gas shift reaction on the four catalysts in the fresh Pt/Rh/BaO/CeO_2 family. The feed contained 5% CO_2 and 5000 ppm H_2.

Fixed NO_x Storage Experiments. A series of experiments were carried out with the intent to "fix" the amount of NO_x stored on the catalyst samples to focus on differences in the regeneration features. Figure 9 shows the data from storage experiments in which two different catalysts having the same precious metal and oxide loadings (Pt/BaO and Pt/CeO_2; see Table 1) were exposed to the same feed mixture of NO (500 ppm) in O_2 (5%), and the same temperature (300 °C). Figure 9a (top panel) shows the breakthrough of NO and NO_2 and 9b (bottom panel) reports the trapping efficiency (eq 2) as a function of storage time. These particular experiments show the notable differences between a good storage catalyst (Pt/BaO) and an inferior one (Pt/CeO_2). Although the two catalysts achieve comparable NO oxidation conversions, as evidenced by the unreacted NO effluent concentrations at long times, the short-time transient behaviors are quite different. The NO oxidation conversion depends primarily on the feed conditions, fixed in both experiments, as well as the exposed Pt area and dispersion, essentially identical (by design) for the two samples. Regarding the short-time features, NO and NO_2 break through only after a few seconds for Pt/CeO_2 but do not appear until the ~50 s for Pt/BaO. This difference clearly shows the disparity in the NO_x storage on the two catalysts. Figure 9b shows that in order to store the same prescribed amount of NO_x (1.65×10^{-5} mol), 45 s is required for the Pt/BaO, compared with 60 s for the Pt/CeO_2. The corresponding instantaneous trapping efficiencies were 100% and 75% for Pt/BaO and Pt/CeO_2, respectively.

Notable differences were obtained for the catalysts during the regeneration of the fixed amount of stored NO_x. Consider first the Pt/Rh/BaO/CeO_2 series feed devoid of H_2O or CO_2 (Figure 10). Again, an important feature of these experiments is that regeneration of a fixed amount of NO_x was conducted at a prescribed temperature; that is, a cyclic steady-state is not achieved. The data show the effluent transient profiles of the main species over a protracted 200-s regeneration of the four catalysts initially loaded with 1.65×10^{-5} mol of NO_x. The results for the Pt/BaO catalyst show a small NO_x puff at the beginning of the regeneration, the coappearance of N_2, the delayed appearance of H_2O, and the eventual, simultaneous breakthrough of H_2 and NH_3. The production of N_2 proceeds at a constant level (~230 ppm) until the 40 s mark, at which point the unreacted H_2 and NH_3 appear. This signals the depletion of accessible stored NO_x. Somewhat similar effluent profiles were obtained for the other catalysts with some differences. For example, no effluent NO_x was detected, and slightly higher N_2 plateau concentrations were obtained, as were lower ammonia peak ammonia concentrations. The addition of CeO_2 caused a delay in the appearance of H_2, as we discuss later.

dx.doi.org/10.1021/cs200252r |ACS Catal. 2011, 1, 969–988

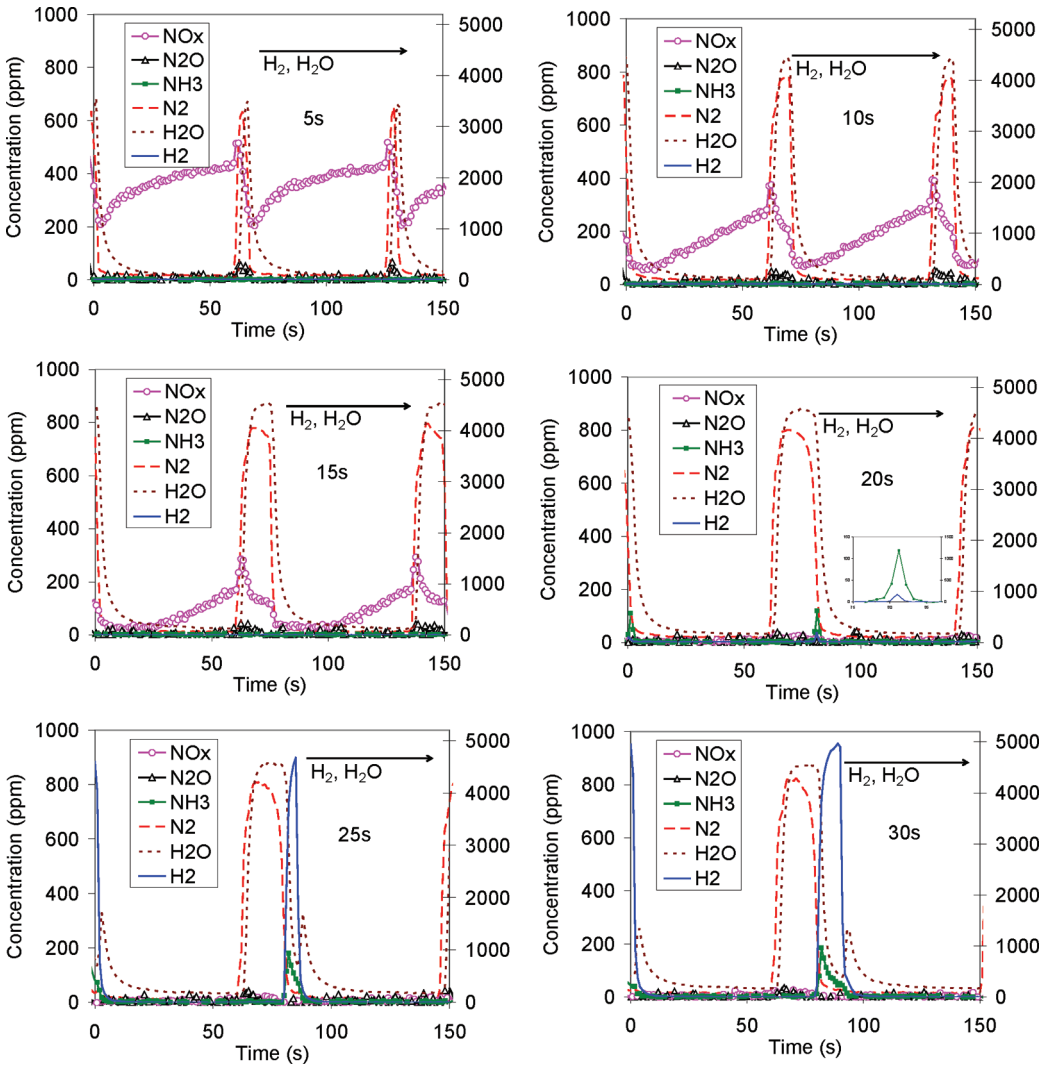

Figure 7. Dependence of instantaneous concentrations of reactants and products during lean-rich cycling on the aged Pt/Rh/BaO/CeO_2 catalyst at 350 °C. The storage feed contained 500 ppm NO in 5% O_2 with a duration of 60 s, whereas the regeneration feed contained 5000 ppm H_2 and had a duration between 5 and 30 s.

A more detailed comparison was carried out for the Pt/BaO and Pt/CeO_2 catalysts using the fixed NO_x protocol. These samples had the same Pt loading, overall washcoat loading, and storage component loading (Table 1). Figure 11 shows the transient profiles at 300 °C, and Figure 12 shows the result of several fixed NO_x experiments carried out at different temperatures. There are several features of interest. The Pt/CeO_2 is an inferior NSR catalyst, as indicated by the significant amount of NO_x released at the start of the regeneration and the much lower N_2 yield. On the basis of the larger H_2O peak and the delayed breakthrough (and prolonged consumption) of H_2, Pt/CeO_2 clearly stores more oxygen. The Pt/BaO also produces much more NH_3. Clearly, although each catalyst stores the same amount of NO_x, the fraction that is actually reduced is much less on the Pt/CeO_2. The effect of temperature on the comparative performance of the two catalysts (Figure 12) indicates that the Pt/CeO_2 is a comparable NSR catalyst only at 150 °C. The differences in the NO_x released, N_2 yield, and NH_3 yield are quite apparent.

Figure 13 reports a detailed breakdown of the selectivity of the N-containing products including the released "NO_x" and the "stored NO_x", that which was not converted or released (estimated by difference). These data provide a complete accounting of the fate of the 1.65×10^{-5} mol of NO_x prestored on the catalysts. The sum of the "NO_x" and "stored NO_x" values is equal to the fraction of unconverted NO_x. Pt/BaO is clearly the superior NSR catalyst in terms of both the fraction converted and the selectivity to N_2. Again, only at 150 °C is Pt/CeO_2 comparable with Pt/BaO.

DISCUSSION

This experimental study compares the storage and reduction performance of a family of Pt/Rh/Ba/Ce monolith catalysts in terms of NO_x conversion and product selectivities using H_2 as the reductant. The catalyst composition, monolith temperature, presence of H_2O and CO_2 in the feed, and regeneration time were systematically varied to identify trends and to elucidate effects. The study also probed the performance of the catalysts in fixed NO_x storage experiments intended to isolate the roles of Rh and CeO_2, especially as they relate to ammonia formation and to the rate-controlling process during regeneration. In this section,

dx.doi.org/10.1021/cs200252r |ACS Catal. 2011, 1, 969–988

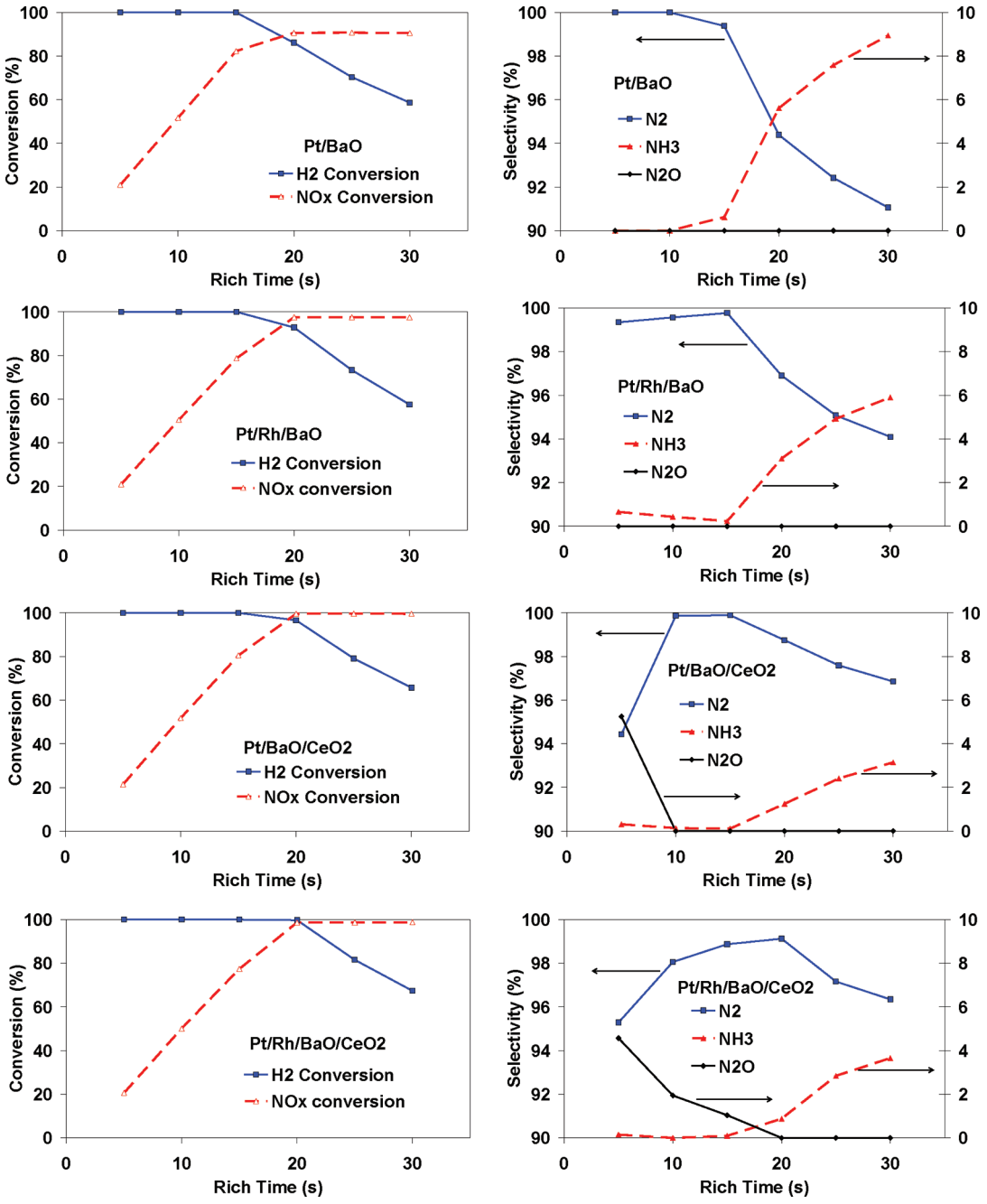

Figure 8. Dependence of cycle-averaged conversion (of H_2 and NO_x) and selectivity (of N_2, N_2O, NH_3) on duration of regeneration (rich time) for four aged catalysts in the Pt/Rh/BaO/CeO_2 family. The temperature is 300 °C, and the storage feed contained 500 ppm NO in 5% O_2 with a duration of 60 s. The regeneration feed contained 5000 ppm H_2.

we analyze some of the major trends that provide some insight about the NSR catalyst performance.

A comparison of the NO oxidation activity of the Pt/Rh/Ba/Ce catalysts helps to elucidate the significance of this reaction during the cycling. The oxidation of NO on Pt proceeds by the sequence of steps:[29]

$$NO + Pt \rightarrow NO{-}Pt \quad (S1)$$

$$O_2 + Pt \leftrightarrow O_2{-}Pt \quad (S2)$$

$$O_2{-}Pt + Pt \leftrightarrow 2O{-}Pt \quad (S3)$$

$$NO{-}Pt + O{-}Pt \leftrightarrow NO_2{-}Pt \quad (S4)$$

$$NO_2{-}Pt \leftrightarrow NO_2 + Pt \quad (S5)$$

S2 is the established rate-determining step.[29] The rate is inhibited by adsorbed NO_2-Pt primarily and NO-Pt secondarily. An added complication is the propensity for Pt to be oxidized by NO_2, which results in slow deactivation. The catalysts in this study exhibited reasonable NO oxidation activity for the feeds either devoid of H_2O and CO_2 or containing CO_2. Rh added to Pt at practical levels (Rh/Pt < 0.1) has a moderate effect on the overall performance of the LNT. Even at the low loading used here

dx.doi.org/10.1021/cs200252r |*ACS Catal.* 2011, 1, 969–988

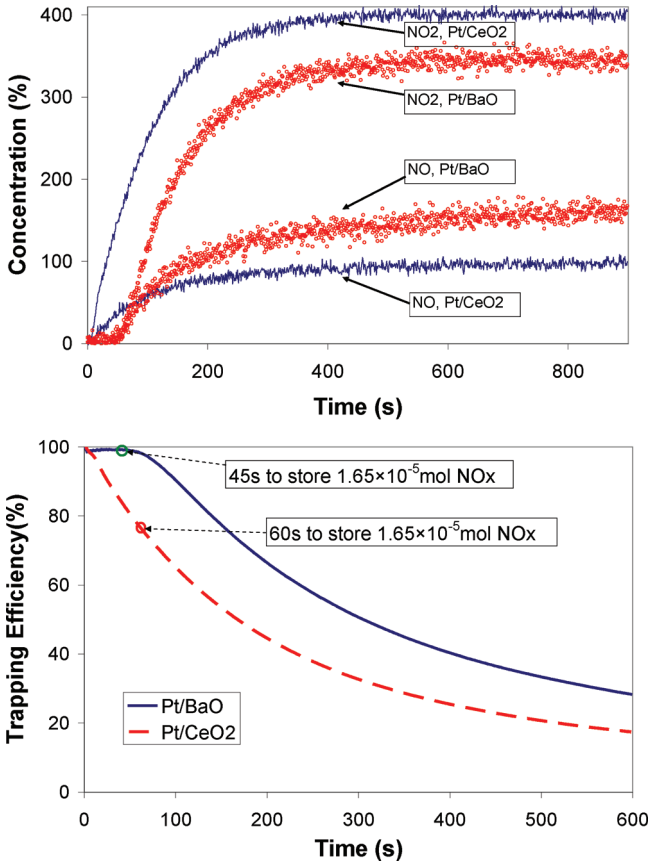

Figure 9. Top panel shows the breakthrough of NO and NO_2 during the exposure of fresh Pt/BaO and Pt/CeO_2 catalysts to a 500 ppm NO in 5% O_2 mixture at 300 °C. Bottom panel shows the calculated NO_x trapping efficiencies.

(Rh/Pt = 0.07), Rh reduced the NO oxidation activity, corroborating the findings of Schmeisser et al.[14] The simplest interpretation is that Rh resides on the Pt crystallites and therefore blocks the more active Pt sites. Rh is also more prone to oxidation than is Pt. The data also indicate that CeO_2 has a slight enhancing effect in the presence of CO_2, but not with the other feeds. These findings differ from those of Schmeisser,[14] who reported a more general enhancement of NO oxidation activity by CeO_2.

The accepted mechanism for lean NO_x storage on Pt/BaO catalysts involves the sequential steps of NO oxidation to NO_2 S1−S5, followed by the reaction of NO_2 with the existing forms of barium (oxide, hydroxide, carbonate), forming a mixture of barium nitrites and barium nitrates. One source of NO_2 is that which is present in the reactor feed; another is the desorbed product of NO oxidation. A fraction of the NO_x is supplied from the Pt crystallites via the Pt/Ba interface: Pt surface species from the NO oxidation, including NO−Pt, O−Pt, and/or NO_2−Pt may spill over to the barium storage phase. Most previous studies have shown that barium nitrate is the primary stored NO_x species.[1−3,23,33,34,36−43] The well-accepted route describing nitrate formation is the disproportionation of NO_2:

$$3NO_2{-}Pt + Ba(OH)_2 \leftrightarrow Ba(NO_3)_2 + NO + H_2O \quad (R2)$$

[Remark: We show $Ba(OH)_2$ rather than BaO, since H_2O is always present during NSR, be it in the feed or as a reaction product. Note that even in experiments without H_2O in the feed, it is present as a product of the stored NO_x reduction during the regeneration, albeit at lower concentrations.] Many studies have shown satisfaction of the disproportionation stoichiometry; that is, 1 NO formed/3 NO_2 consumed.[23,33,39−43] Nova et al.[44] and Prinetto et al.[45] proposed the alternative "nitrite route", which involves NO and O species adsorbed on the Pt:

$$O{-}Pt + Ba(OH)_2 \leftrightarrow BaO_2 + H_2O \quad (S6)$$

$$NO{-}Pt + BaO_2 \leftrightarrow BaO{-}NO_2 \quad (S7)$$

$$NO{-}Pt + BaO{-}NO_2 \leftrightarrow Ba(NO_2)_2 \quad (S8)$$

The nitrites can be oxidized by gas phase O_2 and NO_2 or surface O and NO_2, forming barium nitrate; for example,

$$O_2 + Ba(NO_2)_2 \leftrightarrow Ba(NO_3)_2 \quad (S9)$$

In the presence of water, the oxidation of NO to NO_2 is inhibited. Water is known to adsorb on Pt at low temperature,[43] so it is reasonable to expect that this leads to the blockage of sites on the Pt surface for adsorption of oxygen, the established rate-limiting step for Pt-catalyzed NO oxidation.[29] But the inhibition does not translate to a decrease in the NO_x storage or NO_x conversion during lean−rich cycling (Figure 2). To explain this apparent inconsistency, first consider the effect of water on NO oxidation and NO_x storage. In the presence of H_2O, the NO oxidation chemistry is more complex and faces additional kinetic obstacles. Adsorbed hydroxyls formed by the adsorption of H_2O[46] initiate chemistry mimicking the chemistry of nitrous and nitric acid formation:

$$H_2O + Pt \leftrightarrow OH{-}Pt + H{-}Pt \quad (S10)$$

$$NO{-}Pt + OH{-}Pt \leftrightarrow HNO_2{-}Pt + Pt \quad (S11)$$

$$NO_2{-}Pt + OH{-}Pt \leftrightarrow HNO_3{-}Pt + Pt \quad (S12)$$

$$NO{-}Pt + HNO_3{-}Pt \leftrightarrow HNO_2{-}Pt + NO_2{-}Pt \quad (S13)$$

S13 is a known heterogeneous reaction that occurs on the surface of particulates in polluted atmospheres.[47] Ross and De Vore[48] showed that HNO_3 persists on alumina for temperatures up to 300 °C. It has also been proposed as a key reaction during NH_3-based SCR.[49] These additional species may also spill over to the storage phase; for example, nitrous and nitric acid may form nitrites and nitrates, respectively:

$$2HNO_2{-}Pt + Ba(OH)_2 \leftrightarrow Ba(NO_2)_2 + 2H_2O + 2Pt \quad (S14)$$

$$2HNO_3{-}Pt + Ba(OH)_2 \leftrightarrow Ba(NO_3)_3 + 2H_2O + 3Pt \quad (S15)$$

In effect, the complex mixture of surface species blocks sites for O_2 adsorption, resulting in a reduction in the rate of NO oxidation of NO to NO_2. Given that NO_2 formation is a key step for NO_x storage, it may be expected that H_2O would also reduce the NO_x storage capacity. However, the data during cycling (Figure 2) and results from previous studies[16] do not show a decrease in NO_x storage. Indeed, the formation and

dx.doi.org/10.1021/cs200252r |ACS Catal. 2011, 1, 969–988

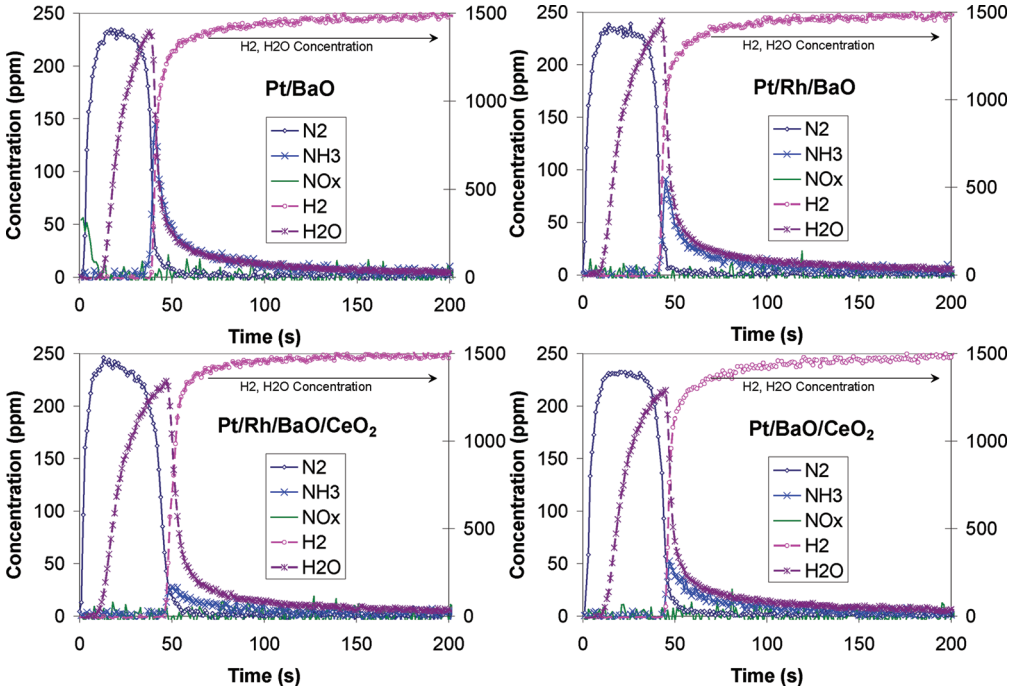

Figure 10. Instantaneous temporal profiles of the reactant and product concentrations for the four fresh catalysts during regeneration with 1500 ppm H_2 at 300 °C. About 1.65×10^{-5} mol of NO_x were stored on each catalyst before regeneration.

spillover of surface species such as HNO_2, HNO_3, etc. may enhance the storage.

The reduced production of NO_2 also does not translate to a corresponding reduction in the cycle-averaged NO_x conversion; that is, the inhibiting effect of H_2O is largely mitigated. This can be attributed to the scavenging of sorbed species by the H_2 reductant. Otherwise, the presence of water in the feed would also lower the NO_x conversion from its level without water in the feed. H adatoms that are present due to the dissociative adsorption of H_2 readily scavenge adsorbed O adatoms and OH species (reverse of S10), forming H_2O. The scavenging of OH reduces the coverage of surface nitrous and nitric acids S11 and S12. Ultimately, the Pt surface is cleansed of sorbed species that would otherwise block the adsorption of O_2 and NO. In addition, the aforementioned spillover of NO_2, HNO_2, HNO_3, etc. from the Pt crystallites to the barium phase during storage may have an analogous reverse spillover process from the storage phase to Pt during the regeneration.

The effect of CO_2 has a similar disjointed effect: Unlike H_2O, CO_2 adsorption does not significantly reduce the NO oxidation to NO_2, indicating that CO_2 does not block precious metal sites for O_2 adsorption. But there is a drop in the cycle-averaged NO_x conversion, which is more pronounced at lower temperatures. Since the cycling conditions involved a protracted 30 s regeneration, the decreased NO_x conversion in the presence of CO_2 has mainly to do with the NO_x storage features of the catalyst. These results are in line with previous works that have shown that the uptake of NO_x on barium carbonate is much less effective than on barium hydroxide. Lietti et al.[15] were among the first to report such an effect on NO_x storage, with the reactivity decreasing in the order of BaO > $Ba(OH)_2$ > $BaCO_3$. $BaCO_3$ is more stable than BaO/$Ba(OH)_2$, and therefore, the storage of NO_x is lower at a particular temperature and $NO/NO_2/O_2$ feed composition. Another potential effect is the reaction of CO_2 with H_2 via the

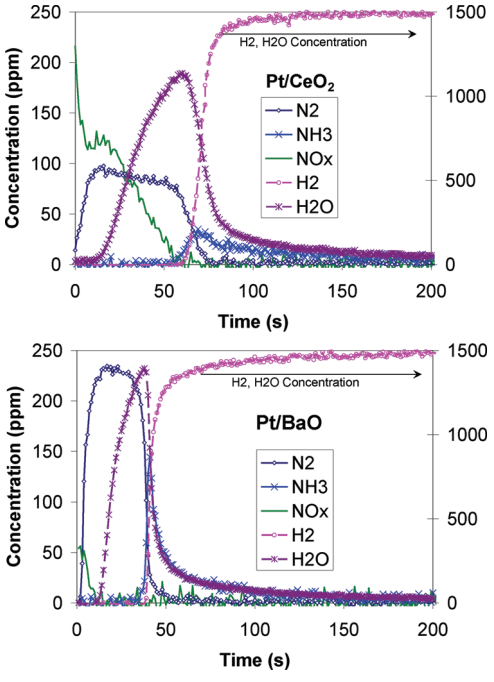

Figure 11. Instantaneous temporal profiles of the reactant and product concentrations for the fresh Pt/BaO and Pt/CeO_2 and catalysts during regeneration at 300 °C. About 1.65×10^{-5} mol NO_x were initially stored on each catalyst before exposure to 1500 ppm H_2.

reverse water gas shift reaction (rWGS). This effect is most important at moderate temperatures. The steady-state data (Figure 6) showed that the reaction commences at about 250 °C for a feed containing 5% CO_2 and 5000 ppm H_2. The conversion of a fraction of the H_2 to CO means that a more

dx.doi.org/10.1021/cs200252r |ACS Catal. 2011, 1, 969–988

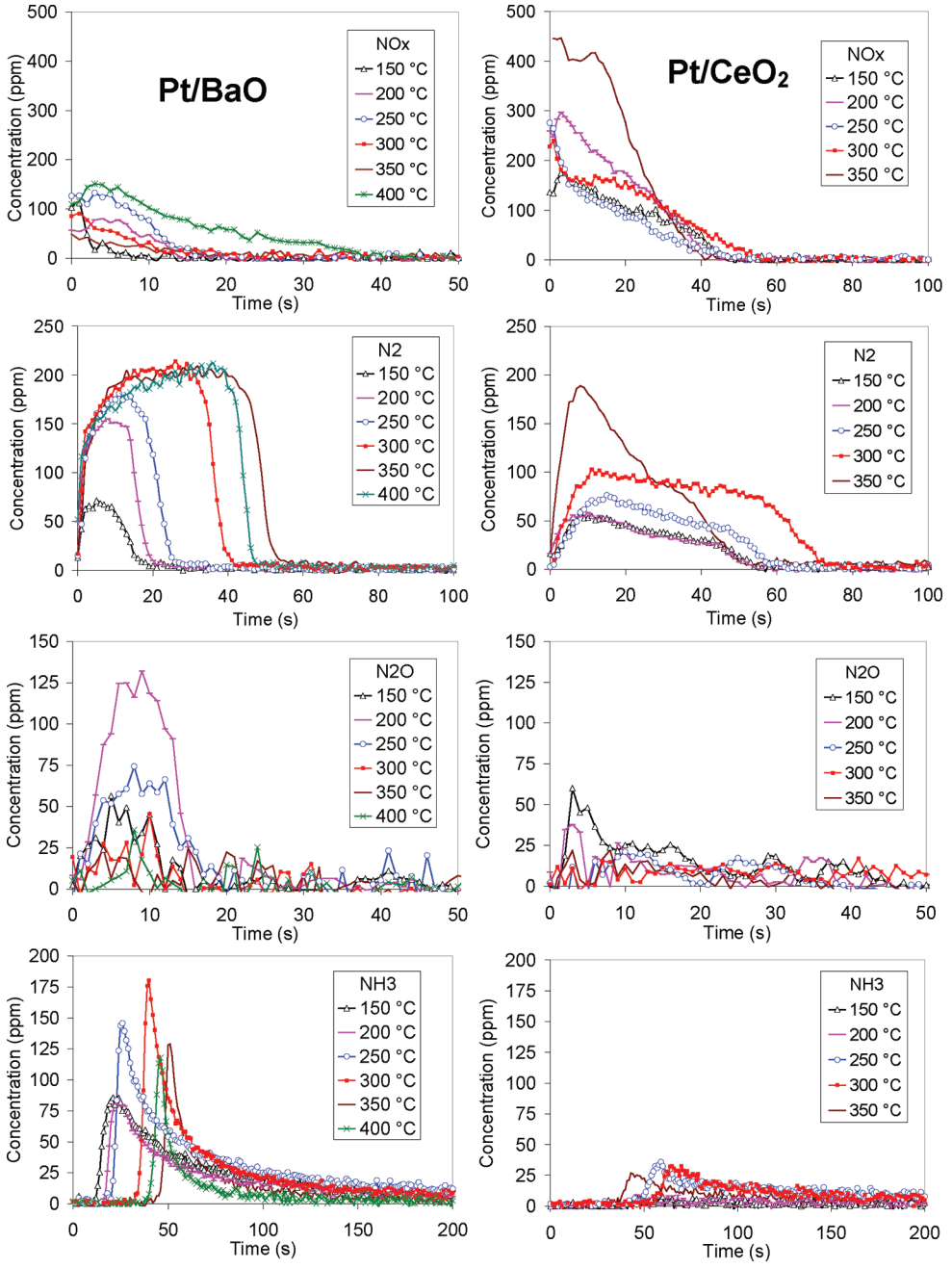

Figure 12. Instantaneous temporal profiles of the reactant and product concentrations for the aged Pt/BaO (left column) and Pt/CeO_2 (right column) catalysts during regeneration at several temperatures. About 1.65×10^{-5} mol of NO_x were initially stored before exposure to 1500 ppm H_2.

effective reductant (H_2) is supplanted by a less effective reductant (CO). The light-off temperature of CO oxidation (by O_2) on Pt is close to 200 °C, whereas for H_2 oxidation, light-off occurs at much lower temperatures.[26] The reductant effect diminishes at higher temperature (>350 °C), conditions for which the reactivities of CO and H_2 converge.

The sensitivity to CO_2 concentration may be only of fundamental interest, since it is always present in relatively high concentrations in vehicle exhaust. Nevertheless, the effect of CO_2 on the N-containing product distribution during cycling deserves some consideration because of the interesting trends. The results in Figures 3 and 4 show that the addition of CO_2 at higher temperatures (>300 °C) leads to an increase in the NH_3 selectivity at the expense of a decrease in the N_2 selectivity. At lower temperatures (<250 °C), CO_2 effects an increase in the N_2O selectivity, primarily at the expense of a decrease in the NH_3 selectivity. This is more pronounced on the catalysts without Rh. The selectivity trends at higher temperatures suggest that the existence of the more stable $BaCO_3$ inhibits storage of NO_x during the lean phase; as a result, NH_3 generated upstream in the reactor during the rich phase encounters less stored NO_x downstream. This results in an increase in the net NH_3 produced in the presence of CO_2. On the other hand, the selectivity trend at lower temperature suggests that CO_2 inhibits NH_3 formation in favor of N_2O. This is an unusual shift in product distribution because NH_3 is a "deep reduction" product, whereas N_2O is a

dx.doi.org/10.1021/cs200252r |ACS Catal. 2011, 1, 969–988

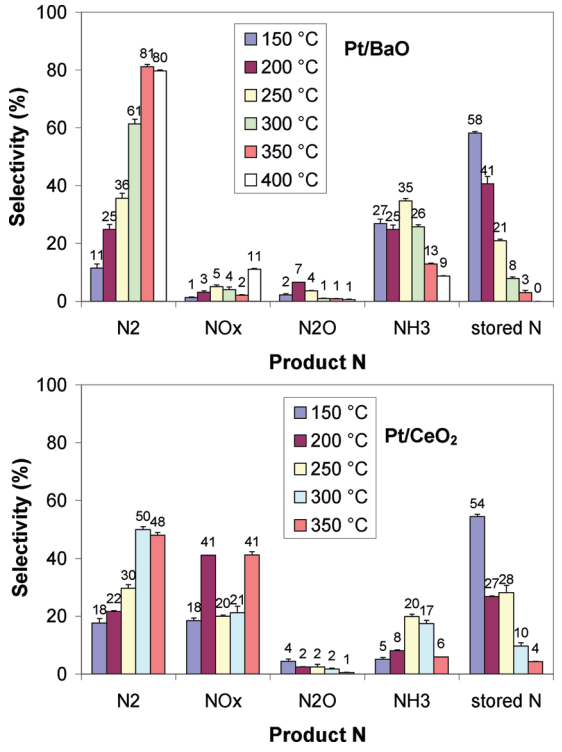

Figure 13. Integral distribution of the reactant and product concentrations for the aged Pt/BaO (top) and Pt/CeO_2 (bottom) catalysts during regeneration at several temperatures. About 1.65×10^{-5} mol of NO_x were initially stored before exposure to 1500 ppm H_2.

"partial reduction" product. Adsorption by CO_2, followed by the formation of a carboxyl intermediate (COOH−Pt) through reaction with H−Pt, and subsequent dissociation to CO−Pt and OH−Pt could reduce the fraction of vacant sites on the Pt. Grabow et al.[50] have shown the involvement of H adatoms during water gas shift on Pt. A surface covered with a significant fraction of CO−Pt could inhibit NH_3 formation while enhancing N_2O formation. NH_3 formation involves the following steps:

$$NO + Pt \leftrightarrow NO{-}Pt$$

$$NO{-}Pt + Pt \leftrightarrow N{-}Pt + O{-}Pt$$

$$H_2 + 2Pt \leftrightarrow 2H{-}Pt$$

$$N{-}Pt + 3H{-}Pt \leftrightarrow NH_3 + 4Pt$$

Up to five Pt sites are required. In contrast, N_2O formation can occur by the following steps:

$$NO + Pt \leftrightarrow NO{-}Pt$$

$$2NO{-}Pt \leftrightarrow N_2O + O{-}Pt + Pt$$

Here, only two Pt sites are required, and is more likely on a crowded surface. Additional experiments are needed to fully elucidate these secondary selectivity trends.

A simple analysis of the ratio of hydrogen to NO_x consumed enables one to determine the form of stored NO_x; that is, nitrite or nitrate. Consider the experiment with the aged Pt/BaO catalyst without CO_2 or H_2O in the feed. During the 30 s regeneration, 0.22 mmol of H_2 is supplied. The H_2 conversion is 55%, NO_x conversion is 90%, and the selectivity to N_2 is 94% (Figure 8). The amount of NO_x stored is 0.170 mmol NO_x/g wc, which corresponds to 0.022 mmol of N for the 130 mg of washcoated sample. For the stated conversions, the ratio of hydrogen to nitrogen reacted is $(H/N)_r = 6.11$ during one cycle. In the absence of CO_2, the following N_2 producing reactions occur:

Table 3. The Fraction of NO_x Contained in "NO_x Puff"

		temperature (°C)					
		150	200	250	300	350	400
Pt/BaO	w/o CO_2/H_2O	0.03	0.03	0.02	0.01	0.01	0.04
	w/H_2O	0.03	0.05	0.06	0.05	0.04	0.06
	w/CO_2	0.02	0.07	0.11	0.16	0.15	0.17
Pt/BaO/CeO_2	w/o CO_2/H_2O	0.08	0.04	0.01	0.00	0.00	0.01
	w/H_2O	0.01	0.01	0.02	0.03	0.02	0.04
	w/CO_2	0.04	0.06	0.05	0.04	0.04	0.06
Pt/Rh/BaO	w/o CO_2/H_2O	0.06	0.07	0.03	0.01	0.00	0.02
	w/H_2O	0.01	0.02	0.04	0.04	0.03	0.04
	w/CO_2	0.02	0.07	0.07	0.05	0.05	0.08
Pt/Rh/BaO/CeO_2	w/o CO_2/H_2O	0.06	0.04	0.02	0.01	0.00	0.02
	w/H_2O	0.00	0.01	0.01	0.02	0.01	0.03
	w/CO_2	0.05	0.09	0.06	0.03	0.04	0.08

$$3H_2 + Ba(NO_2)_2 \rightarrow Ba(OH)_2 + 2H_2O + N_2 \quad (R3)$$

$$5H_2 + Ba(NO_2)_2 \rightarrow Ba(OH)_2 + 4H_2O + N_2 \quad (R4)$$

The additional reaction between H_2 and chemisorbed oxygen also occurs:

$$H_2 + O{-}Pt \rightarrow H_2O + Pt \quad (R5)$$

We estimate that 0.008 mmol of H_2 reacts via R5 if all of the exposed Pt atoms are occupied by one oxygen atom. Thus, the corrected $(H/N)_r$ is equal to 5.70. This value is slightly higher than if all of the NO_x was stored as nitrate; that is, the stoichiometry of R4 is H/N = 5. If we account for the small amount of NO_x converted to NH_3, then we can conclude that NO_x is primarily stored in the form of nitrate.

The regeneration chemistry is obviously much more complicated than the above three global reactions involving H_2 and stored NO_x. Their utility is in calculating overall consumption ratios and assessing selectivity trends. Clearly, complex chemistry occurs as the H_2 adsorbs and reacts with OH−Pt, O−Pt, NO−Pt, etc. on the precious metal crystallites. Several groups have attempted to describe the regeneration chemistry with much larger sets of global reactions or microkinetic steps.[2,16,18,51−54] Our intent is not to delve into those findings here, but rather, to try to explain some of the trends as they relate to the formation of NH_3; the roles of Rh and CeO_2; and, to a lesser extent, effects due to CO_2 and H_2O, underpinned by previous mechanistic and kinetic modeling studies.

At the initial phase of the regeneration, some NO_x may leave the reactor unconverted. The magnitude of this "NO_x puff" can be determined from the transient data by subtracting the moles of NO_x converted from the moles of NO_x stored. Table 3 provides

dx.doi.org/10.1021/cs200252r |ACS Catal. 2011, 1, 969–988

the NO_x puff fraction, normalized by the NO_x fed for a given set of operating conditions. The fractional values are generally less than 0.10. Thus, the majority of the stored NO_x is converted. That said, the data show that the NO_x puff is largest for the Pt/BaO catalyst and when CO_2 is in the feed. In the absence of H_2O/CO_2, the NO_x puff fraction decreased with temperature over the range of 150−350 °C, achieving a minimum at 350 °C, and then increased between 350 and 400 °C. Theis et al.[35] pointed out that the NO_x puff is affected by several factors, including the amount of NO_x stored, the LNT volume, temperature, amount of oxygen storage capacity, richness of purge, purge flow rate, etc. Later, Epling et al.[55] pointed out that the magnitude of the NO_x puff is a function of four primary processes: namely, the reductant feed rate, nitrate decomposition, OSC consumption, and NO_x reduction. That the largest puff occurs when CO_2 is in the feed conveys the increased decomposition rate of the stored nitrate in the presence of the more stable $BaCO_3$. The variation with temperature exemplifies the balance between the nitrate decomposition and reduction at the interface between the precious metal and storage functions. The presence of ceria generally reduces the magnitude of the puff, which conveys its participant as a NO_x storage material.

As mentioned in the Introduction, the lean NO_x trap may serve as a stand-alone NO_x reduction reactor or as a combined NO_x reducer/NH_3 generator in the tandem LNT/SCR application. The performance target of the former is high N_2 yield, whereas for the latter, the NH_3 yield must be high enough so that any NO_x that slips from the LNT during the next storage cycle is eliminated through reaction with said NH_3 trapped in the SCR. In general, Pt/BaO catalyst exhibits the highest cycle-averaged NH_3 selectivity for all of the catalysts (Figure 4). The findings are generally consistent with trends reported previously by Clayton et al.[26,56] Our findings in the current study show that the addition of Rh and CeO_2 reduces the production of NH_3, a preferred result for the LNT application but an undesired result for the LNT/SCR application. The data show that the N_2 selectivity increases monotonically with temperature, exceeding 80% for T > 350 °C. This is consistent with an increased N−O bond scission rate.[57−59] The addition of Rh certainly enhances this trend. The trends corroborate the pioneering work of Schlatter and Taylor[6] who showed that Rh is more effective than Pt in converting NO to N_2 rather than NH_3 under steady-state conditions, although the difference diminished with aging of the catalysts. The argument put forth by the authors is that Rh is effective in catalyzing NH_3 removal, particularly when O_2 is absent, compared with Pt. Clayton et al.[56] showed for a Pt/BaO catalyst that the N_2 selectivity decreased for T > 400 °C; they explained this trend to be the result of a reduced NO_x storage and therefore reduced NH_3 oxidation in the downstream part of the reactor. This regime was not encountered in the current study. In general, for a fixed set of conditions, a feed that is devoid of CO_2 and H_2O gave the highest N_2 selectivity for each of the catalysts. The only exception was the results obtained for the Pt/Ba/Ce catalyst, for which a higher N_2 selectivity was obtained in the presence of H_2O. The presence of CO_2 in the feed led to reduced N_2 selectivity for all of the catalysts and T > 200 °C. One explanation mentioned earlier regards the increased stability of $BaCO_3$, which gives reduced NO_x storage and, therefore, a lower conversion of NH_3 to N_2.

The addition of CeO_2 should be avoided in a LNT/SCR application. Undoubtedly, the higher oxygen storage capacity of the CeO_2 promotes the oxidation of the NH_3 intermediate. This feature was previously reported by Ji et al.[8] The NH_3 selectivity is highest in the lower temperature range (T < 250 °C) in the presence of H_2O and in the higher temperature range (T > 300 °C) in the presence of CO_2. The higher temperature behavior may be attributed to the higher H_2/NO_x ratio that results when a fixed supply of reductant encounters a lower level of NO_x storage. The lower temperature behavior is attributed to the reduced consumption of NH_3 through reaction with NO_x stored downstream in the reactor.[26,33,60,61] Another factor is that the extent of the endothermic dehydrogenation of NH_3 is less at a lower temperature.[56]

Although not as significant a product as NH_3, a few points and discernible trends for the N_2O selectivity data deserve attention. Previous studies have shown that N_2O forms by the combination of NO and N surface species on a clean Pt surface.[57−59] In the NO + H_2 reaction system, the product distribution comprising N_2, N_2O, and NH_3 depends on the temperature and the NO/H_2 ratio.[26,62] Generally, the N_2O selectivity decreases monotonically with increasing temperature.[58] As the temperature increases, the rates of NO bond scission and NO desorption increase. This leads to lower conversion to N_2O. During the initial part of the regeneration phase of the NSR cycle, H_2 scavenges adsorbed O on the Pt, generating H_2O. Once sites are freed-up, this enables the spillover of stored NO_x species onto the Pt, and subsequently, surface catalysis occurs between the H, NO, and N adspecies. Under these transient conditions, the instantaneous NO/H ratio has an important bearing on the product selectivity. The gas phase shifts from net oxidizing (lean) to net reducing (rich). Consequently, the reaction between NO and H_2 on the Pt first produces H_2O (H_2 + O−Pt), then N_2O, N_2, and NH_3. This helps to explain the initial appearance of N_2O.

Another pathway proposed by Partridge et al.[63] involves reaction between NH_3 formed upstream and adsorbed NO that is supplied by the stored NO_x downstream. Steady-state reaction between gas phase NH_3 and NO on Pt results in a mixture of N_2, N_2O, and NO, the selectivities of which depend on temperature.[56] Whether H_2 or NH_3 reacts with stored NO_x in the downstream part of the reactor depends on which of the two species is at the leading part of the traveling reductant front. Bhatia et al.[64] noted that some data indicate NH_3 leading the H_2 front; this may enable NH_3 to react with the stored NO_x spilling over to the Pt. On the other hand, Clayton et al.[60] showed that when a mixture of H_2 and NH_3 and NO are contacted with Pt, NH_3 does not react until all of the H_2 is consumed. Further experiments are needed to finalize the N_2O formation mechanism. Finally, it is notable that the catalysts containing ceria produce more N_2O. A possible explanation is that the consumption of reductant by the stored oxygen consumes reductant that would otherwise serve to reduce the N_2O to N_2.

The results show how the systematic variation in the regeneration time can divide the cyclic operation into reductant and NO_x-limited regimes. The cycle-averaged selectivities of the main N-containing products convey the importance of the cycle-averaged H_2/NO_x feed ratio (Figure 8). In general, an increase in the regeneration (rich) time increases the ammonia selectivity at the expense of the N_2 selectivity. The N_2 selectivity exhibits a monotonic decreasing dependence on the regeneration time for the Pt/BaO catalyst. On the other hand, for the CeO_2-containing catalysts, there is a nonmonotonic dependence of the N_2 selectivity, with a maximum occurring at an intermediate rich time. N_2O is favored under reductant-limited conditions (short rich times). For a fixed regeneration time, the fraction of NH_3 is

highest for the Pt/BaO catalyst. For example, an ~20 s regeneration results in high NO_x and H_2 conversion, and the NH_3 selectivity is 3−5%. This compares to a much lower selectivity of 1% for the BaO/CeO_2-containing catalysts. The higher NO_x-to-N_2 selectivity is due in part to the increased storage provided by the CeO_2 and NO bond scission activity provided by the Rh. The oxygen storage capacity of CeO_2 has two effects. First, the effective H_2/NO_x ratio in the front of the reactor, which would tend to decrease the amount of NH_3 formed. The second effect is an expected increase in the extent of ammonia oxidation downstream. The addition of Rh to the Pt/BaO is slightly detrimental to NH_3 formation. Rh is known to be an effective N−O bond scission catalyst, which favors N_2 formation, as shown by Schlatter and Taylor.[6] Indeed, as mentioned earlier, the earlier versions of the catalytic converter produced too much NH_3; it was only after the addition of CeO_2 and Rh that these levels came down.

The fixed storage experiments provide a more detailed assessment of the regeneration chemistry and rates. By prestoring the same amount of NO_x, one can avoid differences in the storage dynamics and capacities of different catalysts. A prescribed amount of stored NO_x is obtained by flowing a mixture of NO and O_2 over a catalyst and measuring the trapping efficiency. For example, Figure 9. shows the results for the Pt/BaO and Pt/CeO_2 catalysts. The same amount of NO_x (16.5 μmol) was stored on each catalyst, although this amount was achieved much more quickly on the Pt/BaO catalyst (45 s) than the Pt/CeO_2 catalyst (60 s). Then each catalyst was exposed to the same regeneration conditions.

The main trends in the species profiles during the fixed storage experiments were similar for each catalyst under the conditions in Figure 10 (monolith temperature of 300 °C, GHSV of 60 K h^{-1}): N_2 was produced at a nearly constant concentration for the initial part of the regeneration, and H_2O appeared after a short lag and peaked at about the same point in time that the N_2 concentration dropped and the H_2 broke through. Unreacted NO_x was measured at the start of the regeneration (such as for Pt/BaO). The intermediate product NH_3 appeared and reached a peak at essentially the same point as the H_2 breakthrough. Both the NH_3 and H_2O gradually declined over the remaining 150 s of regeneration. Most of these trends are consistent with previous lean−rich cycling on NSR catalysts.[26,56] The N_2 plateau and belated NH_3 breakthrough features are consistent with the established role of NH_3 as an intermediate reductant that reacts with stored NO_x downstream of its generation location.[56,60,61] At 300 °C, the regeneration is sufficiently fast that the feed rate of H_2 is the limiting process: H_2 moves through the reactor as a moving front and NH_3 moves through as a moving front of finite duration. The differences among the four catalysts for the particular experiments in Figure 10 are minor. For example, only the Pt/BaO catalyst had a measurable breakthrough of unreacted NO_x ("NO_x puff"). Another difference was the somewhat longer breakthrough time for H_2 for the CeO_2-containing catalysts. This is attributed to the reaction between H_2 and stored oxygen.

A direct assessment of the effect of CeO_2 on the regeneration was made by comparing the behavior of Pt/BaO and Pt/CeO_2 catalysts that had the same loading of the storage component (12.7 wt %) and precious metal (2.36 wt %). Figure 9 compares the storage dynamic of these two catalysts, and Figure 11 compares the "fixed-storage" regeneration results. Differences in the product distribution versus time of exposure to a feed containing 1500 ppm H_2 (in Ar) are noteworthy: The Pt/CeO_2 catalyst has a much higher H_2 consumption, H_2O production, and unreacted NO_x breakthrough and lower N_2 and NH_3 production. These differences are mainly the result of differences in the oxygen storage capacity of the two catalysts. The impact of the stored oxygen is seen in the H_2 consumption and water production. The H_2 does not appear until ~65 s into the regeneration period for the Pt/CeO_2 compared with ~40 s for Pt/BaO. About 0.084 mmol of H_2 react on the Pt/CeO_2, compared with 0.054 mmol for the Pt/BaO. This is also seen in the much larger generation of water for the former compared with the latter. At the start of the regeneration, O adatoms are likely adsorbed on the Pt crystallites of the catalysts. However, because of the higher oxygen storage on the CeO_2 compared with the BaO, an additional 0.03 mmol of H_2 are consumed. This amount exceeds the ~0.008 mmol of exposed Pt on the Pt/CeO_2 catalyst, underscoring the fact the source of the oxygen is the ceria phase. Possible reactions include either the reduction of ceria (7) or the reaction between H_2 and O adatoms on the ceria:

$$H_2 + 2CeO_2 \rightarrow Ce_2O_3 + H_2O \quad \text{(R6)}$$

$$H_2 + CeO_2 - O \rightarrow CeO_2 + H_2O \quad \text{(R7)}$$

Reactions R7 and R6 comprise a simplified depiction of the Pt-catalyzed reaction between hydrogen and a surface oxygen supplied by the oxidized ceria.

An examination of the instantaneous NO_x conversion, shown in Figure 13 and calculated from the protracted 900 s regeneration experiments (Figure 12), helps to elucidate the dynamic behavior differences between the Pt/BaO and Pt/CeO_2 catalysts. The data show that the Pt/CeO_2 is notably inferior to the Pt/BaO. In particular, both the "NO_x puff" and unreacted NO_x are significantly larger. For example, at 250 °C, the Pt/CeO_2 data show that 20% of the stored NO_x is released and 28% does not react; that is, a rather low 52% conversion. This compares with 5% and 21%, respectively, for the Pt/BaO catalyst, which is a 74% conversion. At 350 °C, the stored NO_x conversion on the Pt/CeO_2 is not that much higher (55%) but is nearly complete for the Pt/BaO (98%). That the NO_x release occurs mostly during the initial part of the regeneration suggests that the reduction is slower than the rate of desorption of NO from the Pt surface or the rate of NO spillover from the proximal storage sites. These findings suggest that NO_x stored in the cerium phase, presumably as a mixture of nitrites ($Ce(NO_2)_3$) and nitrates ($Ce(NO_3)_3$), is less stable than the corresponding stored NO_x species in the barium phase, in line with the works of Crocker and co-workers,[8−10] among others.

The dependence of the instantaneous stored NO_x conversion on time over a range of temperatures helps to identify the rate controlling regimes and to amplify the differences in the regeneration features of the Pt/BaO and Pt/CeO_2 catalysts (Figure 14). For $T \geq 200$ °C, the NO_x conversion on the Pt/BaO catalyst follows a line of constant slope during the initial phase of the regeneration. The time period for which the linear regime exists increases with temperature. Clayton et al.[27] reported similar results for Pt/BaO having Pt dispersions between 3 and 50% and identified this to be a reductant feed-limited regime in which the conversion is essentially independent of temperature. The H_2 moves through the monolith as a front until breakthrough with the NO_x conversion rate determined by entirely by the H_2 feed rate. The transition, which occurs earlier at lower temperatures, is

dx.doi.org/10.1021/cs200252r |ACS Catal. 2011, 1, 969–988

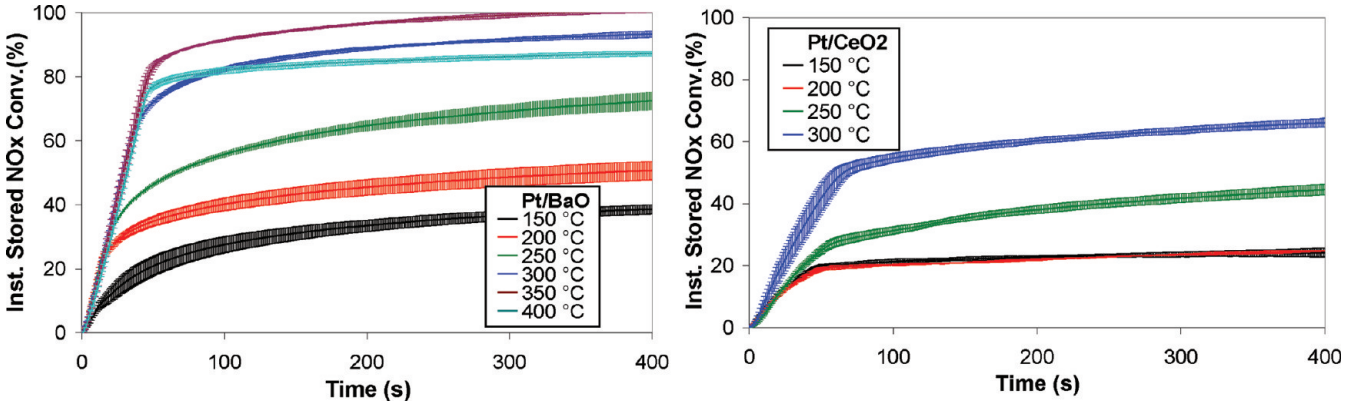

Figure 14. Instantaneous conversion of stored NO_x as a function of time for the aged Pt/CeO_2 and Pt/BaO catalysts. About 1.65×10^{-5} mol of NO_x were stored on each catalyst before regeneration with 1500 ppm H_2.

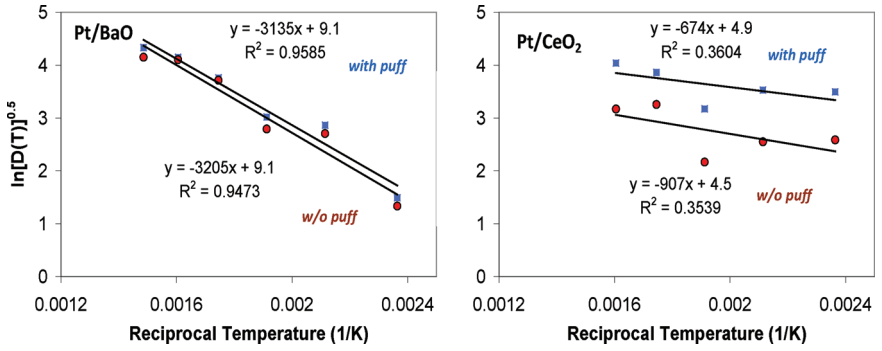

Figure 15. Dependence of logarithm of the square root of the diffusivity on the reciprocal temperature for the Pt/BaO (left panel) and Pt/CeO_2 (right panel) catalysts (data from Figure 14 analyzed).

to a regime limited at least in part by the transport (supply) of stored NO_x to the active Pt sites.[56] It is noted that at the highest temperature (400 °C), there is a slight reduction in the asymptotic NO_x conversion from the 350 °C results. This is due to the decomposition of the stored NO_x; that is, the rate of stored NO_x decomposition exceeds the aforementioned transport process, resulting in a lower instantaneous conversion.

Here, we follow the approach taken by Bhatia et al.[65] in evaluating the "long time" data for the Pt/BaO and Pt/CeO_2 catalysts. Under strictly solid-state diffusion control, the instantaneous conversion scales with time according to

$$X(t) \approx \sqrt{D(T)\, t} \tag{13}$$

where D is a temperature-dependent diffusion coefficient. In the regime, the slope of $\ln(X(t))$ versus $\ln(t)$ gives a line of slope of 0.5 and an intercept proportional to $\ln[(D(T))^{1/2}]$. The latter quantity, in turn, can be plotted as a function of the reciprocal temperature, assuming satisfaction of the Arrhenius equation. This gives another line that has a slope equal to $E_D/2R$, where E_D is the activation energy of the activated solid-state diffusion of NO_x.

Figure 15a reports the results of the Arrhenius analysis for the Pt/BaO catalyst using the conversion data in Figure 14. Analyses were carried out of the NO_x conversion excluding (Figure 14) and including the unreacted NO_x puff. E_D is estimated to be 52−53 kJ/mol with little difference whether the NO_x puff is included or not. The data show that the regeneration rate becomes nearly independent of time at higher temperature; that is, slope of $\ln(X(t))$ vs $\ln(t) \rightarrow 0$. On the other hand, Bhatia et al.[65] analyzed similar data for a sintered Pt/BaO catalyst having a Pt dispersion of only 3% and found a good fit of eq 13 over the entire regeneration. They estimated E_D to be 75 kJ/mol. Kumar et al.[66] corroborated this estimate in independent TAP experiments employing ^{15}NO and the same low dispersion catalyst, estimating E_D to be 80 kJ/mol. The lower valued estimated in the current study suggests that the NO_x conversion is not limited solely by a diffusion process. Since the Pt dispersion is ~50%, the effective diffusion length is much shorter, on the order of a few nanometers, so the stored NO_x is much more accessible to the catalytic sites. Apparently, another process prevents the complete regeneration of stored NO_x despite the rather high Pt dispersion. One possibility could be that diffusion of nitrates is dependent on the concentration of stored NO_x. That is, as the concentration of stored NO_x decreases, the mobility of the diffusing nitrate species decreases. Other explanations may involve an evolving textural feature. Additional experiments are needed to fully resolve this complex system.

The transient regeneration features of the Pt/CeO_2 catalyst have some similarities but noted differences compared with Pt/BaO catalyst. Like the Pt/BaO catalyst, the stored NO_x conversion is an increasing function of the temperature. But unlike the Pt/BaO catalyst, this regime is encountered only in an intermediate temperature range (200−300 °C). Another difference

for the Pt/CeO_2 is an apparent lower, nonzero conversion limit at lower temperature; that is, a decrease in the temperature below 200 °C does not lead to any further decrease in conversion. These features suggest that a fraction of the stored NO_x on the Pt/CeO_2 is essentially kinetically inaccessible. The fraction that is accessible appears to be responsible for the better performance of the Pt/CeO_2 catalyst at low temperature. Finally, at temperatures above 300 °C, the Pt/CeO_2 catalyst has much lower stability compared with the Pt/BaO catalyst. The activation energy analysis for the Pt/CeO_2 catalyst (Figure 15b) shows considerably more scatter than for the Pt/BaO catalyst. We estimate E_D to be between 11.2 (including the NO_x puff) and 15.1 (excluding the puff) over the entire temperature range (150−350 °C). The considerably lower estimate of E_D for the Pt/CeO_2 catalyst is evidence for a much less stable stored NO_x species compared with the Pt/BaO catalyst and is consistent with previous studies[8−12] that suggested that cerium nitrates and nitrites are less stable, which accounts for the somewhat higher NO_x reduction at low to moderate temperatures.

CONCLUSIONS

In this study, we have compared the storage and reduction features of a family of $Pt/Rh/BaO/CeO_2/Al_2O_3$ washcoated monolith catalysts using H_2 as the reductant. The study builds on the established understanding of the Pt/BaO model NSR catalyst by assessing the roles of Rh and CeO_2 as additional components during the storage and reduction processes. In addition, specific issues presented by engine exhaust species H_2O and CO_2 are explored in the context of the catalyst comparisons, such as the conversion of H_2 to CO via the reverse water gas shift reaction being more pronounced for the sample containing Rh and CeO_2. Particular attention is placed on the generation and consumption of NH_3 and how the addition of Rh and CeO_2 affect this balance. Most of the observed trends are interpreted in terms of the likely reaction pathways and transport processes. Some of the main new findings from this approach are summarized below.

The addition of CeO_2 at a loading on par with that of BaO has important effects on the overall performance. The main effect is due primarily to the oxygen storage capacity of CeO_2 and secondarily to the incremental NO_x storage capacity. The oxygen storage increases the consumption of reductant during the regeneration, including the fed H_2 and the intermediate product NH_3. The latter NH_3 oxidation increases the overall selectivity to N_2. Fixed NO_x storage experiments clearly exhibit the inferior NSR performance of Pt/CeO_2 compared to Pt/BaO. On the other hand, the coexistence of BaO and CeO_2 has an overall beneficial effect on the NSR performance, but again, the increase in NO_x conversion comes at the expense of additional H_2 consumption. The fixed NO_x experiments help to identify the rate-controlling process during regeneration. Both the Pt/BaO and Pt/CeO_2 catalysts exhibit a feed-rate-limited state at the beginning of regeneration, shifting to a regime in which the supply of NO_x to the active sites is limited in part by an activated solid state diffusion process. The data indicate that a fraction of stored NO_x cannot be regenerated, suggesting that the mobility of stored NO_x is inhibited by chemical or textural factors.

The observed effects of H_2O and CO_2 in the feed are in good agreement with literature findings for Pt/BaO, although the extent of certain effects may be impacted by Rh, CeO_2, or both. Water inhibits the oxidation of NO on each catalyst, but the cycle-averaged NO_x conversion is largely unaffected. CeO_2 slightly enhances NO oxidation in the presence of CO_2. On the other hand, CO_2 has only a minor effect on the conversion during steady state NO oxidation but significantly inhibits the conversion during cyclic storage and reduction. This effect is attributed to the higher stability of $BaCO_3$ compared with $BaO/Ba(OH)_2$ as well as to the conversion of H_2 to the less effective reductant CO via reverse water gas shift chemistry. Both Rh and CeO_2 increase the overall activity of this conversion.

Finally, this study shows how the particular LNT application directly affects the selection of the lean NO_x trap catalyst composition. For the conventional stand-alone intended to convert NO_x to N_2, a fully formulated trap containing Pt, BaO, Rh, and CeO_2 makes sense. This catalyst gives the highest NO_x conversion and N_2 selectivity. On the other hand, the combined LNT/SCR application requires that the LNT efficiently generate NH_3. The performance of such a device should not contain CeO_2 or Rh if a high net NH_3 generation rate is desired, notwithstanding other benefits of Rh/CeO_2, such as sulfur tolerance and durability.

AUTHOR INFORMATION

Corresponding Author
*E-mail: mharold@uh.edu.

ACKNOWLEDGMENT

This study was funded by the National Science Foundation (CT50730824). We thank Dr. C. Z. Wan from BASF Catalysts (Iselin, NJ) for providing the model catalysts for this study. The authors appreciate the helpful suggestions of the reviewers in providing some additional explanation of the trends in the data. This report was prepared as an account of work sponsored by an agency of the United States Government. Neither the United States Government nor any agency thereof nor any of their employees makes any warranty, express or implied, or assumes any legal liability or responsibility for the accuracy, completeness, or usefulness of any information, apparatus, product, or process disclosed, or represents that its use would not infringe privately owned rights.

REFERENCES

(1) Epling, W. S.; Campbell, L. E.; Yezerets, A.; Currier, N. W.; Parks, Ii, J. E. *Catal. Rev.—Sci. Eng.* **2004**, *46* (2), 163–245.
(2) Güthenke, A.; Chatterjee, D.; Weibel, M.; Krutzsch, B.; Kocí, P.; Marek, M.; Nova, I.; Tronconi, E. *Advances in Chemical Engineering*; Guy, B. M., Ed.; Academic Press: New York, 2007; Vol. 33, pp 103−211, 280−283.
(3) Roy, S.; Baiker, A. *Chem. Rev.* **2009**, *109* (9), 4054–4091.
(4) Theis, J.; Ura, J.; McCabe, R. W. *SAE Transactions* **2007**, 2007-01-1055.
(5) Gandhi, H. S.; Graham, G. W.; McCabe, R. W. *J. Catal.* **2003**, *216* (1−2), 433–442.
(6) Schlatter, J. C.; Taylor, K. C. *J. Catal.* **1977**, *49*, 42–50.
(7) Theis, J.; Ura, J.; Coralski, C., Jr.; Jen, H.; Thanasin, E.; Graves, Y.; Takami, A.; Yamada, H.; Miyoshi, S. *SAE Transactions* **2003**, 23−37.
(8) Ji, Y.; Toops, T.; Crocker, M. *Catal. Lett.* **2007**, *119* (3), 257–264.
(9) Ji, Y.; Choi, J.-S.; Toops, T. J.; Crocker, M.; Naseri, M. *Catal. Today* **2008**, *136* (1−2), 146–155.
(10) Ji, Y.; Fisk, C.; Easterling, V.; Graham, U.; Poole, A.; Crocker, M.; Choi, J.-S.; Partridge, W.; Wilson, K. *Catal. Today* **2010**, *151* (3−4), 362–375.

(11) Casapu, M.; Grunwaldt, J. D.; Maciejewski, M.; Krumeich, F.; Baiker, A.; Wittrock, M.; Eckhoff, S. *Appl. Catal., B* **2008**, *78* (3−4), 288–300.
(12) Yoshida, H.; Yazawa, Y.; Takagi, N.; Satsuma, A.; Tanaka, T.; Yoshida, S.; Hattori, T. *J. Synchrotron Radiat.* **1999**, *6* (3), 471–473.
(13) Martin, D.; Duprez, D. *J. Phys. Chem.* **1996**, *100* (22), 9429–9438.
(14) Schmeisser, V.; Riva Perez, J.; Tuttlies, U.; Eigenberger, G. *Top. Catal.* **2007**, *42/43*, 15–19.
(15) Lietti, L.; Forzatti, P.; Nova, I.; Tronconi, E. *J. Catal.* **2001**, *204* (1), 175–191.
(16) Epling, W. S.; Peden, C. H. F.; Szanyi, J. *J. Phys. Chem. C* **2008**, *112* (29), 10952–10959.
(17) Theis, J.; Jen, H.; McCabe, R. W.; Sharma, M.; Balakotaiah, V.; Harold, M. P. *SAE Transactions* **2006**, 2006-01-1067.
(18) Lindholm, A.; Currier, N. W.; Fridell, E.; Yezerets, A.; Olsson, L. *Appl. Catal., B* **2007**, *75* (1−2), 78–87.
(19) Scholz, C. M. L.; Nauta, K. M.; de Croon, M. H. J. M.; Schouten, J. C. *Chem. Eng. Sci.* **2008**, *63* (11), 2843–2855.
(20) Lindholm, A.; Currier, N. W.; Li, J.; Yezerets, A.; Olsson, L. *J. Catal.* **2008**, *258* (1), 273–288.
(21) Schmeisser, V.; Tuttlies, U.; Eigenberger, G. *Top. Catal.* **2007**, *42/43*, 77–81.
(22) Schmeisser, V.; Eigenberger, G.; Nieken, U. *Top. Catal.* **2009**, *52* (13), 1934–1939.
(23) Kabin, K. S.; Khanna, P.; Muncrief, R. L.; Medhekar, V.; Harold, M. P. *Catal. Today* **2006**, *114* (1), 72–85.
(24) Clayton, R. D. Ph.D Dissertation, University of Houston, Houston, TX, 2008.
(25) Olsson, L.; Fridell, E. *J. Catal.* **2002**, *210* (2), 340–353.
(26) Clayton, R. D.; Harold, M. P.; Balakotaiah, V. *AIChE J.* **2009**, *55* (3), 687–700.
(27) Clayton, R. D.; Harold, M. P.; Balakotaiah, V.; Wan, C. Z. *Appl. Catal., B* **2009**, *90* (3−4), 662–676.
(28) Olsson, L.; Westerberg, B.; Persson, H.; Fridell, E.; Skoglundh, M.; Andersson, B. *J. Phys. Chem. B* **1999**, *103* (47), 10433–10439.
(29) Bhatia, D.; McCabe, R. W.; Harold, M. P.; Balakotaiah, V. *J. Catal.* **2009**, *266* (1), 106–119.
(30) Muncrief, R. L.; Khanna, P.; Kabin, K. S.; Harold, M. P. *Catal. Today* **2004**, *98* (3), 393–402.
(31) Breen, J. P.; Rioche, C.; Burch, R.; Hardacre, C.; Meunier, F. C. *Appl. Catal., B* **2007**, *72* (1−2), 178–186.
(32) Abdulhamid, H.; Fridell, E.; Skoglundh, M. *Appl. Catal., B* **2006**, *62* (3−4), 319–328.
(33) Kabin, K. S.; Muncrief, R. L.; Harold, M. P. *Catal. Today* **2004**, *96* (1−2), 79–89.
(34) Fridell, E.; Skoglundh, M.; Westerberg, B.; Johansson, S.; Smedler, G. *J. Catal.* **1999**, *183* (2), 196–209.
(35) Theis, J.; Ura, J. A.; Li, J. J.; Surnilla, G. G.; Roth, J. M.; Goralski, C. T. *SAE Transactions* **2003**, 2003-01-1159.
(36) Cant, N. W.; Patterson, M. J. *Catal. Today* **2002**, *73* (3−4), 271–278.
(37) Broqvist, P.; Gronbeck, H.; Fridell, E.; Panas, I. *Catal. Today* **2004**, *96* (1−2), 71–78.
(38) Despres, J.; Koebel, M.; Kröcher, O.; Elsener, M.; Wokaun, A. *Appl. Catal., B* **2003**, *43* (4), 389–395.
(39) Mahzoul, H.; Brilhac, J. F.; Gilot, P. *Appl. Catal., B* **1999**, *20* (1), 47–55.
(40) Yi, C.-W.; Kwak, J. H.; Szanyi, J. *J. Phys. Chem. C* **2007**, *111* (42), 15299–15305.
(41) Nova, I.; Castoldi, L.; Lietti, L.; Tronconi, E.; Forzatti, P.; Prinetto, F.; Ghiotti, G. *J. Catal.* **2004**, *222* (2), 377–388.
(42) Scotti, A.; Nova, I.; Tronconi, E.; Castoldi, L.; Lietti, L.; Forzatti, P. *Ind. Eng. Chem. Res.* **2004**, *43* (16), 4522–4534.
(43) Epling, W. S.; Parks, J. E.; Campbell, G. C.; Yezerets, A.; Currier, N. W.; Campbell, L. E. *Catal. Today* **2004**, *96* (1−2), 21–30.
(44) Nova, I.; Castoldi, L.; Prinetto, F.; Dal Santo, V.; Lietti, L.; Tronconi, E.; Forzatti, P.; Ghiotti, G.; Psaro, R.; Recchia, S. *Top. Catal.* **2004**, *30/31* (1−4), 181–186.
(45) Prinetto, F.; Ghiotti, G.; Nova, I.; Castoldi, L.; Lietti, L.; Tronconi, E.; Forzatti, P. *Phys. Chem. Chem. Phys.* **2003**, *5* (20), 4428–4434.
(46) Daschbach, J. L.; Peden, B. M.; Smith, R. S.; Kay, B. D. *J. Chem. Phys.* **2004**, *120* (3), 1516–1523.
(47) Rivera-Figueroa, A. M.; Sumner, A. L.; Finlayson-Pitts, B. J. *Environ. Sci. Technol.* **2003**, *37* (3), 548–554.
(48) Ross, M. W.; DeVore, T. C. *J. Phys. Chem. A* **2008**, *112*, 6609–6620.
(49) Nova, I.; Ciardelli, C.; Tronconi, E.; Chatterjee, D.; Bandl-Konrad, B. *Catal. Today* **2006**, *114* (1), 3–12.
(50) Grabow, L.; Gokhale, A. A.; Evans, S. T.; Dumesic, J. A.; Mavrikakis, M. *J. Phys. Chem.* **2008**, *114* (1), 3–12.
(51) Forzatti, P.; Lietti, L.; Gabrielli, N. *Appl. Catal., B* **2010**, *99* (1−2), 145–155.
(52) Kocí, P.; Plát, F.; Stepánek, J.; Kubícek, M.; Marek, M. *Catal. Today* **2008**, *137* (2−4), 253–260.
(53) Larson, R. S.; Pihl, J. A.; Kalyana Chakravarthy, V.; Toops, T. J.; Daw, C. S. *Catal. Today* **2008**, *136* (1−2), 104–120.
(54) Xu, J.; Harold, M. P.; Balakotaiah, V. *Appl. Catal., B* **2009**, *89* (1−2), 73–86.
(55) Epling, W. S.; Yezerets, A.; Currier, N. W. *Appl. Catal., B* **2007**, *74* (1−2), 117–129.
(56) Clayton, R. D.; Harold, M. P.; Balakotaiah, V. *Appl. Catal., B* **2008**, *84* (3−4), 616–630.
(57) Burch, R.; Millington, P. J. *Catal. Today* **1995**, *26* (2), 185–206.
(58) Burch, R.; Millington, P. J.; Walker, A. P. *Appl. Catal., B* **1994**, *4* (1), 65–94.
(59) Medhekar, V.; Balakotaiah, V.; Harold, M. P. *Catal. Today* **2007**, *121* (3−4), 226–236.
(60) Pihl, J. A.; Parks, J. E.; Daw, C. S.; Root, T. W. *SAE Tech. Pap. Ser.* **2006**, 2006-01-3441.
(61) Cumaranatunge, L.; Mulla, S. S.; Yezerets, A.; Currier, N. W.; Delgass, W. N.; Ribeiro, F. H. *J. Catal.* **2007**, *246* (1), 29–34.
(62) Clayton, R. D.; Harold, M. P.; Balakotaiah, V. *Appl. Catal., B* **2008**, *81* (3−4), 161–181.
(63) Partridge, W. P.; Choi, J.-S. Presentation at 2011 CLEERS meeting, Dearborn, MI, 2011.
(64) Bhatia, D.; Clayton, R. D.; Harold, M. P.; Balakotaiah, V. *Catal. Today* **2009**, *147* (Suppl. 1), S250–S256.
(65) Bhatia, D.; Harold, M. P.; Balakotaiah, V. *Catal. Today* **2010**, *151* (3−4), 314–329.
(66) Kumar, A.; Harold, M. P.; Balakotaiah, V. *Ind. Eng. Chem. Res.* **2010**, *49* (21), 10334–10340.